
On the Validity of Mean Value Engine Models During Transient Operation

Alain Chevalier

Ford Motor Co.

Martin Müller

Delphi Automotive System

Elbert Hendricks

Technical University of Denmark

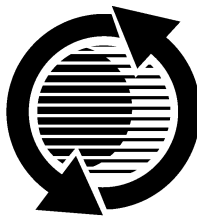
Reprinted From: **Modeling of SI Engines**
(SP-1511)

The appearance of this ISSN code at the bottom of this page indicates SAE's consent that copies of the paper may be made for personal or internal use of specific clients. This consent is given on the condition, however, that the copier pay a \$7.00 per article copy fee through the Copyright Clearance Center, Inc. Operations Center, 222 Rosewood Drive, Danvers, MA 01923 for copying beyond that permitted by Sections 107 or 108 of the U.S. Copyright Law. This consent does not extend to other kinds of copying such as copying for general distribution, for advertising or promotional purposes, for creating new collective works, or for resale.

SAE routinely stocks printed papers for a period of three years following date of publication. Direct your orders to SAE Customer Sales and Satisfaction Department.

Quantity reprint rates can be obtained from the Customer Sales and Satisfaction Department.

To request permission to reprint a technical paper or permission to use copyrighted SAE publications in other works, contact the SAE Publications Group.



GLOBAL MOBILITY DATABASE

All SAE papers, standards, and selected books are abstracted and indexed in the Global Mobility Database

No part of this publication may be reproduced in any form, in an electronic retrieval system or otherwise, without the prior written permission of the publisher.

ISSN 0148-7191

Copyright © 2000 Society of Automotive Engineers, Inc.

Positions and opinions advanced in this paper are those of the author(s) and not necessarily those of SAE. The author is solely responsible for the content of the paper. A process is available by which discussions will be printed with the paper if it is published in SAE Transactions. For permission to publish this paper in full or in part, contact the SAE Publications Group.

Persons wishing to submit papers to be considered for presentation or publication through SAE should send the manuscript or a 300 word abstract of a proposed manuscript to: Secretary, Engineering Meetings Board, SAE.

Printed in USA

On the Validity of Mean Value Engine Models During Transient Operation

Alain Chevalier
Ford Motor Co.

Martin Müller
Delphi Automotive System

Elbert Hendricks
Technical University of Denmark

Copyright © 2000 Society of Automotive Engineers, Inc.

ABSTRACT

Because there are no production-type sensors which are able to measure the flow directly at the intake port, it is becoming common practice to use models of varying complexity to infer the port air mass flow from other measurements. Given the tight requirements of modern air/fuel ratio (*AFR*) control strategies, the accuracy of these models needs to be better than ever, during steady-state of course (though λ feedback strategies are by design very robust), but mainly during transient operation. This paper describes why conventional models might be inaccurate during engine transients.

By developing a simulation package (one-dimensional (*1D*) solution of the Navier and Stoke (*NESS*) equations), which can describe complex phenomena such as manifold acoustics (inertial ramming, resonance), heat-transfer, friction, backflow, in-cylinder process, moving valves and throttle, junctions, it is shown that current control models need to be modified if they are to be able to describe port air mass flow with the required accuracy during transient operation. In particular, it is discussed why one should pay more attention to pumping fluctuations, heat transfer and friction. An improved model suitable for control applications is finally proposed. Experimental data are also shown.

1 INTRODUCTION

With the tightening of exhaust emission standards, wide bandwidth control of the *AFR* of spark ignition (*SI*) engines has enjoyed increased interest recently. Most modern *AFR* control strategies are based on the use of dynamic multi-variable nonlinear engine models. The performance of the final controllers usually depends largely on the accuracy of these models. Unfortunately, in many previous *AFR* control related publications, emphasis has been on the control aspect rather than the modeling aspect of the

problem. Especially, often models are accepted as valid control tools provided they are capable of reproducing measured variables such as manifold pressure, throttle air mass flow, etc. But because it is impossible to measure the air mass flow at the intake ports (one of the most important variables in *AFR* control), it has so far been impossible to verify if these engine models are really suitable for tight *AFR* control. One alternative solution, the one elaborated in this work, is to use a model of higher complexity to validate models of lower complexity such as a Mean Value Engine Model (*MVEM*). The results presented here are therefore mainly theoretical and the purpose of the paper is to suggest potential improvements to existing *MVEM*s and to give the reader confidence that these models have the accuracy required for control applications.

The paper is organized in four parts. In the first part, a discussion about why *MVEM*s may need some improvement is given. In the second section, a wave action model developed at the Technical University of Denmark (*DTU*) for the purpose of concurrent testing, is presented briefly. In the third part, simulation results, where the different parts of *MVEM*s are analysed, are presented and improved models are proposed. In the fourth section, one form of the new model is compared to experimental results. The paper is finally ended with some concluding remarks.

2 MOTIVATIONS

The most common (but also the most simple) port air mass flow model is given by the speed-density equation which states that the mass of air flowing into the cylinders equals the volume flow of the engine, times the air density.

Because the engine is not a perfect pump, this flow needs to be corrected by the volumetric efficiency, a non-dimensional coefficient that measures the breathing performance of the engine. This coefficient is usually deduced from *steady-state* measurements: the engine equipped with

a mass air flow (*MAF*) sensor¹, is run at different operating conditions; the measured air mass flow rate, \dot{m}_a , is then normalized with a reference air mass flow rate and the resulting efficiency saved in equation or table form. In principle, it does not matter which reference is used, as long as the same reference is also used in the speed-density equation. Two different references are commonly used, one based on the density of air at ambient conditions (leading to Equations (1) and (2)) and one based on air at intake manifold conditions (leading to Equations (3) and (4)).

$$\eta_{vol}^{amb} = \frac{\dot{m}_a}{\frac{N V_{disp} P_{amb}}{120 r T_{amb}}} \quad (1)$$

$$\dot{m}_{ap} = \eta_{vol}^{amb} \frac{N V_{disp} P_{amb}}{120 r T_{amb}} \quad (2)$$

$$\eta_{vol}^{man} = \frac{\dot{m}_a}{\frac{N V_{disp} P_{man}}{120 r T_{man}}} \quad (3)$$

$$\dot{m}_{ap} = \eta_{vol}^{man} \frac{N V_{disp} P_{man}}{120 r T_{man}} \quad (4)$$

η_{vol}^{amb} and η_{vol}^{man} are referred to as volumetric efficiencies based on ambient conditions and manifold conditions respectively. They mainly depend on engine speed N , intake pressure P_{man} and intake temperature T_{man} . \dot{m}_{ap} is the port air mass flow. P_{amb} and T_{amb} are the ambient pressure and temperature respectively. V_{disp} is the displacement volume of the engine and r the specific gas constant.

Note that even though the speed density equation is calibrated from steady-state engine data, it is also used to estimate port air mass flow during transient operation. In other words, any transient trajectory is assumed to be made up of a series of steady-state operating points. This is of course only an approximation of the real phenomenon, for which equilibrium is not established instantaneously but rather on a time scale which is short compared to other parts of the system.

If the time development of the port air mass flow during transients is rapid, then it makes sense to neglect the dynamics associated with it and to use the approximate instantaneous (algebraic) relationship. However, careful inspection of the physics of engine breathing suggests that the time development of the volumetric efficiency might not be as fast as it first appears. Among the many phenomena affecting engine breathing performance, four are worth mentioning here as they might have a noticeable impact on the speed-density equation during transient operation:

¹The placement of this *MAF* sensor is not important for steady-state measurements, although the accuracy might be improved if the pumping fluctuations are damped out with a settling box mounted in between the sensor and the engine

1. Inertial Effects

Typically, the air that flows through the engine can be accumulated in different volumes of the manifold (plenums). These volumes are often referred to as the capacitances of the induction system. If the air could flow through the engine without any resistance, the filling of the volumes would be instantaneous and the capacitance would have no transient impact. It is the presence of flow resistance (at the valves, at the throttle and elsewhere) combined with the flow capacitance which leads to the primary time dependency of the manifold phenomena as described in the manifold state Equation (5).

$$\dot{P}_{man} = \frac{r T_{man}}{V_{man}} (-\dot{m}_{ap} + \dot{m}_{at}) \quad (5)$$

where V_{man} is the intake manifold volume. The throttle air mass flow, \dot{m}_{at} , is usually approximated as the isentropic flow of air through a converging nozzle discharging into a sudden enlargement. However, in[1], a more physical and more accurate model of the throttle flow is proposed. For the sake of completeness, this model is reproduced in Appendix A.

However, because the mass of air is continuously accelerated/decelerated in the induction system (pumping fluctuations), inertance also plays a dominant role in scavenge performance. During the first part of the induction period, the mass of gas within the intake pipe acquires kinetic energy which is then released during the second part of the induction process. Depending on the geometry of the engine, the valve timing and the operating conditions, this energy balance may be favorable or unfavorable to the breathing performance of the engine.

During steady state operation, this phenomenon, also known as *inertial ramming* [2], is taken into account in the steady-state volumetric efficiency maps. However, the aperiodic flow accelerations/decelerations associated with transient operation (tip-in and tip-out) is typically not included. During the first part of a tip-in, the momentum gained by the column of gas in the intake piping should temporarily decrease induction ramming, while during the last part, the release of this extra momentum should increase ramming (and vice versa during tip out). Due to the complex nature of the processes involved, a quantitative analysis of the transient inertial effects on induction ramming is still not available.

2. Wave Effects

Even if the intake manifold is decomposed into a large number of lumped resistances, capacitances and inductances, which furthers the understanding of the complex phenomena involved in the induction process, this is only an approximation of the manifold which is a true distributed system (made up of an infinite number of resistances, capacitances and inductances distributed along the manifold). A well known consequence of this fact is that signals (such as pressures,

temperatures and flows) will not travel infinitely fast through the induction pipes but rather at a finite speed: the speed of sound. Any disturbance initiated at the boundaries of the manifold (moving piston, moving valves, moving throttle plate, etc.) will therefore travel back and forth along the pipes, experiencing many reflections along the pipes (at open and closed pipes, when reaching sudden area changes, etc.). This is known as the wave effect [3], and is used in modern engines to increase breathing performance at some operating points.

Typically, when the engine is operated in the steady state, waves from different cylinders and from different cycles will travel around and interact in the manifold to finally settle down into a so-called standing wave. The resulting pressure profile in front of the valves during the induction process will significantly influence the charging of the cylinders. Timing of this wave with respect to the induction process is of prime importance.

For example, if a pressure trough arrives at the opened intake valve when piston speed is maximal, the vacuum created by the suction of the piston will be superimposed on the wave trough, thus leading to a standing wave of large amplitude in the intake manifold (especially so when the valve flow becomes sonic at the throat). Phasing of this large wave with the induction process (by tuning the pipe lengths and the valve timing for given engine speeds) may significantly increase the mass of fresh air trapped in the cylinders, especially if the standing wave results in a peak pressure upstream the intake valve just before it closes.

Here again, the impact of the wave effect on the breathing performance of an engine is included in its steady state volumetric efficiency maps. However, when moving from one operating point to another, no standing wave will have the time to settle and therefore excursions of the volumetric efficiency from its steady state value can be expected. In particular, experience shows that it takes several cycles at the same operating point for the wave to settle into a standing wave.

Also not included in the volumetric efficiency maps, is the effect of the waves originating from the rapid opening (closing) of the throttle plate during tip-in (tip-out). Predicting and understanding these complex interacting phenomena during steady state operation has been the interest of many for many years, but the problem is very complex. It is therefore not surprising that there are very few publications on the subject of transient induction ramming (one paper was published on the subject at the 1999 Society for Automotive Engineers (SAE) Congress [4], but it only covers the validity of steady speed volumetric efficiency for engines operated under transient load and constant throttle opening (wide open throttle (*WOT*)), a somewhat restrictive case).

3. Temperature Effects, Heat Transfer and Backflow

While the two previous points concentrate on the validity of steady state volumetric efficiency maps during transient operation, inspection of the speed density equations (Equation (2) or Equation (4)), suggests another source of error when estimating port air mass flow: temperature transients.

Intake temperature is often regarded as a variable with little importance in the speed density equation, because it is always assumed that it can easily and accurately be measured or estimated. A common practice is to measure this temperature with a thermocouple or simply to set it equal to the ambient temperature. While this is certainly a very good assumption during steady state operations, one may wonder if this is still acceptable during transients. In [5], Müller speculates on the fact that the assumption of an isothermal flow in the intake manifold may lead to errors of up to 20% over several cycles in transient, if the flow is rather of the adiabatic type. Note however that Müller was unable to confirm this hypothesis through experiments.

One problem with these experiments is that the temperature variations are expected to happen on a time scale much too short for any conventional temperature sensor (time constant in the order of a second or more) to be able to measure it. At this point, inspection of the energy seems appropriate. During tip-in, the compression of air (which is an exothermic process), releases energy which is either entirely transferred to the manifold wall (isothermal assumption, maximal heat transfer) or entirely transferred back to the air itself (adiabatic assumption, maximal temperature increase) thus increasing temporarily its temperature. The faster the transient, the higher the compression rate and the temperature spike.

In a similar manner, during tip-out, the expansion of air (which is an endothermic process), absorbs energy from the walls (isothermal assumption, maximum heat transfer) or from the air itself (adiabatic assumption, maximum temperature decrease) thus decreasing temporarily the temperature. The shorter the duration of the transient, the higher the expansion rate and the temperature trough. As argued by Müller, the truth probably lies somewhere in between the isothermal and adiabatic processes (in other words, heat transfer between the air and the walls is probably small but not negligible) and this point needs to be investigated further.

Finally, temperature variations may also result if the level of backflow (hot gases temporarily flowing from the cylinders back into the intake runners) also experiences variations during transients. Any temperature excursion long enough to significantly influence the rate of air that flows into the cylinders, but too short to be accurately measured with any conventional sensor, will seriously disturb the port air mass flow estimation problem.

4. Friction

In a lumped parameter description, it is important not to lump all phenomena into too few parameters, otherwise some of the important dynamics might disappear from the model. For engine manifolds, it has been common practice to consider significant only the capacitance of the plenum, the flow resistance of the throttle plate and the flow resistance of the intake port. As mentioned above, the inertance of the pipes may also be important.

In the same way, flow resistance in the pipes, in particular at the junctions between the plenum and the runners, may also influence significantly the time development of the air flow (especially at high engine speed where the flow velocity is high). This can be expected to have a direct impact on the the time required to fill/empty the manifold and therefore on the overall dynamics of the system.

3 WAVE ACTION MODELING

As explained previously, the performance of *MVEM*s for *AFR* control application should primarily be evaluated on the basis of the accuracy of the port air mass flow modeled during transients. Because there are no non-intrusive methods for measuring this variable on a real engine, an alternative solution is to evaluate *MVEM*s against simulations from a model of higher complexity. For more than 35 years now, after the pioneering work of *Benson* [6], the *1D* solution of the Navier and Stoke (*N&S*) equations has been known to give a good description of the unsteady flow (acoustic phenomena) in the pipe system of internal combustion (*IC*) engines, with the possibility to include the effect of friction and heat transfer in the pipes.

Typically, there are two numerical methods for solving these equations.

- In the **Mesh Method of Characteristics** (*MMOC*) of *Benson* ([6],[7],[8]), the set of partial differential equations is transformed into a set of ordinary differential equations (the new dependant variables are known as the Riemann variables) which need to be solved along the characteristics and path lines. Due to linear interpolation between calculated points, the solution offers only first-order approximation to the Riemann variables. Unfortunately, the (nonlinear) transformation back to physical variables such as flows, degrades even further the accuracy of the solution. At *DTU*, a first code for solving the *N&S* equations using the *MMOC* was developed, but the accuracy of the calculated air mass flows was found far below acceptable levels for this project (during steady-state engine operation, the difference between the air flowing in and the air flowing out of the engine could be up to 10%; in other words, the simulated engine was leaking numerically).

- **Finite Difference Methods** (*FDM*) use Taylor's series expansion to approximate time and space derivatives to an arbitrary accuracy. In practice however, these methods are deliberately limited to second order accuracy because they rapidly tend to be numerically oscillatory (due to the presence of 2^{nd} and higher derivatives), thus leading to non-physical overshoots in the presence of pressure or thermal discontinuities. Among the most frequently used *FDM* methods for *IC* engines, the Two-Step Lax-Wendroff (*LW2*) method has gained popularity in the automotive field because, in comparison to the *MMOC* method, it is more accurate (2^{nd} order), easier to implement, faster [9] and more than anything else, it is intrinsically conservative². At *DTU*, the original *MMOC* code was modified to use the *LW2* method instead. The difference of the flows in and out of the engine (during steady-state operation) was decreased to less than 1%. This code was therefore adopted for our transient analysis of *MVEM* models. For the sake of completeness, the code is briefly presented below.

3.1 Two-Step Lax-Wendroff Method

The *N&S* equations describing the unsteady *1D* flow in pipes of varying section, A , in the presence of convective heat transfer, \dot{q} , and wall shear stress ($\tau_w = \frac{1}{2} \rho f u |u|$) are given below. The influence of viscosity and heat conduction are negligible compared to that of friction and convection [11].

$$\begin{aligned} \frac{\partial \rho}{\partial t} + u \frac{\partial \rho}{\partial x} + \rho \frac{\partial u}{\partial x} + \rho u \frac{1}{A} \frac{\partial A}{\partial x} &= 0 \\ \frac{\partial u}{\partial t} + u \frac{\partial u}{\partial x} + \frac{1}{\rho} \frac{\partial P}{\partial x} + \frac{2f}{D} u |u| &= 0 \\ \frac{\partial h_0}{\partial t} + u \frac{\partial h_0}{\partial x} - \frac{1}{\rho} \frac{\partial P}{\partial t} - \dot{q} &= 0 \end{aligned} \quad (6)$$

where h_0 is the stagnation enthalpy

$$h_0 = \frac{\gamma}{\gamma - 1} \frac{P}{\rho} + \frac{u^2}{2} \quad (7)$$

for an ideal gas. f is the friction factor, u the local velocity, P the local pressure and ρ the local density. For an ideal gas

$$\rho = \frac{P}{rT} \quad (8)$$

The two independent variables are x , the pipe abscissa, and t , the time.

The system of Equation (6) is rearranged in a system of

²Satisfies the continuity equations better. This is one of the requirements of the method developed by *Lax and Wendroff* [10] which only applies to systems of conservation laws, such as the one described by the *N&S* equations.

conservation laws, suitable for the *LW2* method.

$$\begin{aligned} \frac{\partial \rho}{\partial t} + \frac{\partial}{\partial x}(\rho u) + \rho u \frac{1}{A} \frac{\partial A}{\partial x} &= 0 \\ \frac{\partial}{\partial t}(\rho u) + \frac{\partial}{\partial x}(\rho u^2 + P) + \\ \rho u^2 \frac{1}{A} \frac{\partial A}{\partial x} + \frac{2f}{D} \rho u |u| &= 0 \\ \frac{\partial}{\partial t} \left(\frac{1}{\gamma - 1} P + \rho \frac{u^2}{2} \right) + \\ \frac{\partial}{\partial x} \left(u \left(\frac{\gamma}{\gamma - 1} P + \rho \frac{u^2}{2} \right) \right) - \\ \rho \dot{q} + \left(\frac{\gamma}{\gamma - 1} P + \rho \frac{u^2}{2} \right) u \frac{1}{A} \frac{\partial A}{\partial x} &= 0 \end{aligned} \quad (9)$$

Or, in vector form

$$\frac{\partial W}{\partial t} + \frac{\partial F}{\partial x} + C = 0 \quad (10)$$

where

$$W = W(x, t) = \begin{pmatrix} \rho \\ \rho u \\ \frac{1}{\gamma - 1} P + \rho \frac{u^2}{2} \end{pmatrix} \quad (11)$$

$$F = F(W) = \begin{pmatrix} \rho u \\ \rho u^2 + P \\ u \left(\frac{\gamma}{\gamma - 1} P + \rho \frac{u^2}{2} \right) \end{pmatrix} \quad (12)$$

$$C = C(W) = \begin{pmatrix} \rho u \\ \rho u^2 \\ u \left(\frac{\gamma}{\gamma - 1} P + \rho \frac{u^2}{2} \right) \end{pmatrix} \frac{1}{A} \frac{\partial A}{\partial x} + \begin{pmatrix} 0 \\ \frac{2f}{D} \rho u |u| \\ -\rho \dot{q} \end{pmatrix} \quad (13)$$

Since ρ , u and P can be expressed as the elements of W ,

$$\begin{aligned} \rho &= W(1) \\ u &= \frac{W(2)}{W(1)} \\ P &= (\gamma - 1) \left(W(3) - \frac{1}{2} \frac{W(2)^2}{W(1)} \right) \end{aligned} \quad (14)$$

F and C are also vector functions of W .

Equation (10) is solved for W according to the method of *Lax and Wendroff* in two steps:

1st step

$$\begin{aligned} W_{i+\frac{1}{2}}^{n+\frac{1}{2}} &= \frac{1}{2} (W_{i+1}^n + W_i^n) - \frac{\Delta t}{2 \Delta x} (F_{i+1}^n + F_i^n) \\ &\quad - \frac{\Delta t}{4} (C_{i+1}^n + C_i^n) \end{aligned} \quad (15)$$

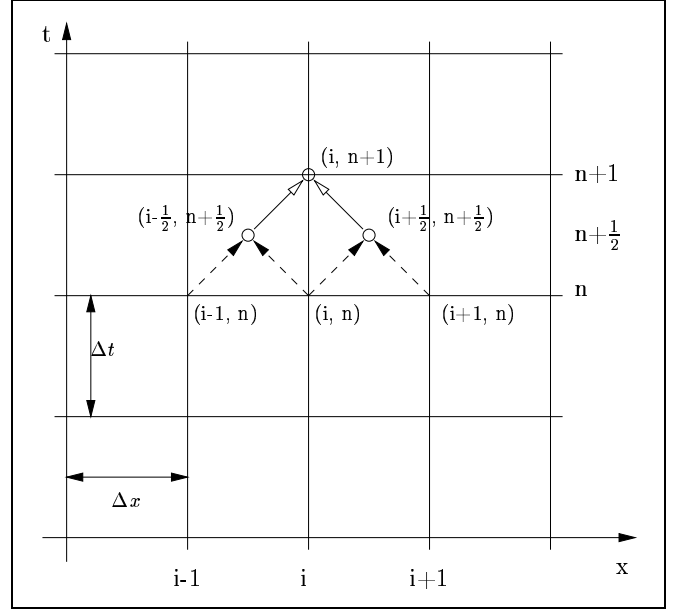


Figure 1: Space-time (x - t) mesh grid for the Two-Step Lax-Wendroff (*LW2*) method.

2nd step

$$\begin{aligned} W_i^{n+1} &= W_i^n - \frac{\Delta t}{\Delta x} (F_{i+\frac{1}{2}}^{n+\frac{1}{2}} - F_{i-\frac{1}{2}}^{n+\frac{1}{2}}) \\ &\quad - \frac{\Delta t}{2} (C_{i+\frac{1}{2}}^{n+\frac{1}{2}} + C_{i-\frac{1}{2}}^{n+\frac{1}{2}}) \end{aligned} \quad (16)$$

where the subscripts indicate the normalized position, and the superscripts the normalized time of the corresponding grid-point (see Figure 1). Δx is the grid size (increment of x), and Δt the time step.

As suggested by *Benson* [7], assuming that the Reynold's analogy for friction and heat transfer [12] applies to non-steady flows, a simple expression for convective heat transfer can be derived

$$\dot{q} = \frac{2f c_p |u|}{D} (T_w - T) \quad (17)$$

where T_w is the local wall temperature, D is the local pipe diameter and c_p the specific heat at constant pressure. The friction factor, f is taken from experimental tables [13]. In [14], different friction factors are tested and $f = 0.004$ appears to be a suitable value.

3.2 Boundary Conditions

Finding and solving the equations at the boundaries is usually tedious. Typically, for each boundary, four regions should be considered. Supersonic flow, subsonic flow, subsonic backflow and supersonic backflow. For each of these regions, the relevant equations which describe the corresponding phenomena should be derived and a numerically stable and efficient scheme for solving this set of (implicit) equations should be developed. Special attention should be paid at the region boundaries where the code should

provide for a smooth and stable crossing from one region to the other (for example from flow to backflow). Because the Mesh Method of Characteristics provides a straight forward interpretation of acoustics phenomena³, it is used to solve the boundary conditions (only at the pipe ends; in the rest of the pipes, the *LW2* method outlined above is used).

A detailed discussion of the boundary conditions used in this work is outside the scope of this paper and only the most important boundary conditions will be discussed, briefly, below.

3.2.1 Valves

Valves are modeled in a manner similar to that proposed by *Pichard* [15]. A description more suitable for numerical treatment can be found in *Daneshyar* [16].

For flows from the cylinder into the pipe, the model considers the gas to flow isentropically from the cylinder to a throat and assumes constant pressure between the throat and the cross section of the pipe (any head loss is implicitly included in the throat area). This assumption applies as long as the flow at the throat is subsonic. When the flow becomes sonic at the throat, the constant pressure assumption is replaced by the condition of unity Mach number at the throat.

For flows from the pipe into the cylinder, the model considers the gas to flow isentropically from the pipe to a throat and assumes constant pressure between the throat and the cylinder (again, any head loss is implicitly included in the throat area). This assumption applies as long as the flow at the throat is subsonic. When the flow becomes sonic at the throat, the constant pressure assumption is replaced by the condition of unity Mach number at the throat.

Closed valves are treated as closed ends, and the only condition to be considered is zero flow velocity at the valves.

Usually, the normalized throat area (also known as the discharge coefficient) is found experimentally, so that, for similar upstream and downstream conditions, the valve models above give the same air mass flow as the one measured on the test rig. Because interest is here focussed on in a qualitative analysis of engine modeling, no attempt is made to reproduce specific experimental data. The discharge coefficient used in this work is thus taken directly from [17].

³Information travels along the characteristics lines. Each boundary conditions needs three equations to be solved (non-homentropic flow). Since each characteristics (and/or path) line brings one equation, the remaining equations must be provided by the boundary. This is helpful information, especially for flow reversal or transonic flow at the boundaries.

3.2.2 Cylinder

The instantaneous volume of the cylinders is known and the pressure and temperature are assumed homogeneous inside the cylinders, with stagnation conditions. Mass conservation and energy conservation give two state equations describing the time development of mass and pressure in the cylinders. The temperature follows from the perfect gas equation. Convective heat transfer between the gas and the cylinder walls is also included and the heat transfer coefficient follows the equation of *Woschni* [18].

The programme described in this paper is not intended for combustion modeling, but only for gas exchange process modeling (between exhaust valve opening (*EVO*) and intake valve closing (*IVC*)). However, what happens in the cylinder when all valves are closed (combustion, etc.) does influence the in-cylinder conditions at *EVO* and should, in principle, be considered in the simulation.

In practice, combustion modeling can be quite inaccurate and it is therefore preferable (and sufficient) to initialize the pressure state equation at every *EVO*, according to mapped real engine data. The mass state equation does not need to be initialized since mass conservation is satisfied whether or not combustion occurs. Temperature at *EVO* follows from the perfect gas equation.

3.2.3 Reservoir (plenum)

The pressure and temperature are assumed homogeneous inside the plenums, with stagnation conditions. Mass conservation and energy conservation give two state equations describing the time development of pressure and temperature in the volumes. The temperature follows from the perfect gas equation. Convective heat transfer between the gas and the walls can also be included (although it is set to zero in this work).

3.2.4 Pipe junction

A constant pressure model [8] is used in this work. While more accurate pipe junction models exist ([19], [20]), this model was selected for its simplicity. Because the engine modeled in this work only has branched pipes in the exhaust ducting system, the accuracy of the pipe junction model should have no impact on the current analysis of *MVEMs*.

3.2.5 Throttle plate

The throttle plate is modeled in a manner similar to that proposed by *Benson, et al.* [21]. Given the relatively small dimension of a throttle body (compared to the length of the waves traveling in the pipes), steady flow is assumed within the throttle element. The flow is also assumed to be

adiabatic (no heat transfer) but non-reversible; the pressure loss across the plate is taken as

$$\Delta P = \frac{1}{2} \rho_{up} f_t u_{up}^2 \quad (18)$$

where ρ_{up} and u_{up} are the density and velocity upstream of the throttle. f_t , the pressure loss coefficient, is a mapped function of the throttle position and the Mach number downstream of the throttle, M_{down} . Energy conservation and continuity complete the set of equations necessary to derive the throttle model.

Note that with an appropriate mapping of f_t , the model of Appendix A is completely equivalent to the model of this section. That is, Figure 16 also applies to the throttle air mass flow in the wave action model⁴.

3.3 Choice of the Time Step

The grid increment, Δx , is known a priori (although it can vary as a function of x). The time step, Δt , is chosen automatically (for all steps) so as to guarantee that the Courant-Friedrichs-Lewy stability criterion

$$\frac{\Delta t}{\Delta x} \leq \frac{1}{c + |u|} \quad (19)$$

is satisfied for all mesh points in all pipes. c is the local speed of sound.

3.4 Code Validation

The code was validated with the help of two well documented tests. The first test is the “de Haller” test (a vessel at high initial pressure expands to atmospheric pressure through a straight pipe) for which numerical solutions in the homentropic and non-homentropic cases are provided in [9].

The second test, due to *Blair and Gouldburn*, is closer to a real engine simulation: a rotary valve, driven by a variable speed gearbox, interrupts cyclicly a flow of compressed air. The resulting pulsating flow, which is representative of exhaust engine pulses, is propagated through pipes of different shapes. Experimental results for this apparatus are given in ([14], [22]).

The code presented in this work gave excellent agreement for both of these test examples.

3.5 Model Generation

Even if the code developed at *DTU* is far from being user-friendly (compared to commercial equivalents such

⁴The only difference between the two models is that the model of Section 3.2.5, suitable for non-steady flow simulations, is more detailed than the model of Appendix A, suitable for *MVEM*'s.

as *WAVE* from Ricardo, *GT-Power* from Gamma Technologies or *DYNOMATION* from V.P. Engineering), it is nevertheless very flexible. Any system which needs to be simulated can be constructed from a set of basic blocks: straight pipes, tapered pipes, pipes with user-defined section and wall temperature profiles, open ends, partially-open ends, closed ends, abrupt changes of area, pipe junctions, pressure losses (air-filter, throttle plate, etc.), valves, cylinders, reservoirs.

For transient simulation, a crankshaft dynamics model is also available (including models of the vehicle inertia, gear-box, rolling resistance and aerodynamics resistance). The program is capable of running transient test-cycles as well as automatic steady-state mappings. Figure 17 in Appendix B shows an example of the type of engine that can be modeled. Note however, that the code is not suitable for multi-phase flows.

4 SIMULATION RESULTS

In order to verify some of the concepts behind Mean Value Engine Modeling, the engine of Figure 17 in Appendix B is proposed as a simulation object. The configuration of the intake manifold is typical for European mid to high-class multi-point injection (*MPI*) engines. The exhaust system, which has only a second order influence on the results of this study (which deals with intake manifold modeling) was chosen for its simplicity. The specifications of the engine can be found in the figure itself.

4.1 Steady-state volumetric efficiency

In a former paper by one of the current authors and coauthors [1], it is suggested that “ $\eta_{vol}^{man} P_{man}$ ”⁵ be mapped (as a function of P_{man} and N) instead of η_{vol}^{man} since the former is an almost linear function of P_{man} , and depends only weakly on N . As a consequence, linear interpolation between the grid points introduces only minimum errors.

In order to take into account the possible changes in barometric pressure, P_{amb} , as well as the possible changes in intake manifold temperature, T_{man} , the mapping of “ $\eta_{vol}^{man} \frac{P_{man}}{P_{amb}}$ ” as a function of “ $\frac{P_{man}}{P_{amb}}$ ” and “ $\frac{N}{\sqrt{T_{man}}}$ ”⁶ is proposed as a further improvement of the “ $e_v \cdot p_i$ ” model. It is easy to see that this new variable can be interpreted as the volumetric efficiency based on barometric pressure, P_{amb} ,

⁵In [1], this is referred to as the “ $e_v \cdot p_i$ ” model.

⁶The choice of these two non-dimensional dependant variables comes from non-dimensional analysis [23]. $\frac{P_{man}}{P_{exh}}$ should actually be used instead of $\frac{P_{man}}{P_{amb}}$. However, the exhaust pressure P_{exh} is usually not known and for naturally aspirated engines P_{exh} and P_{man} are closely related. The presence of the term $\sqrt{T_{man}}$ in the denominator of the second variable can easily be justified by the fact that, for a given manifold geometry, the length of the acoustic waves is proportional to $\frac{\sqrt{T_{man}}}{N}$ ($\sqrt{T_{man}} \propto$ speed of sound in the intake manifold).

and manifold temperature, T_{man} ,

$$\eta_{vol}^{P_{amb}, T_{man}} = \eta_{vol}^{m_{an}} \frac{P_{man}}{P_{amb}} = \frac{\dot{m}_a}{\frac{N V_{disp}}{120} \frac{P_{amb}}{r T_{man}}} \quad (20)$$

The corresponding speed-density equation is given in Equation (21).

$$\dot{m}_{ap} = \eta_{vol}^{P_{amb}, T_{man}} \left(\frac{N}{\sqrt{T_{man}}}, \frac{P_{man}}{P_{amb}} \right) \frac{N V_{disp}}{120} \frac{P_{amb}}{r T_{man}} \quad (21)$$

The wave action model (WAM) was used to estimate the steady-state volumetric efficiency map of the engine of Appendix B. In Figure 2 the simulated $\eta_{vol}^{P_{amb}, T_{man}}$ is shown as a function of “ $\frac{P_{man}}{P_{amb}}$ ” for different “ $\frac{N}{\sqrt{T_{man}}}$ ” values. Because the barometric pressure was set to a constant value throughout the simulation, and because T_{man} remains quite constant over the entire operating region, Figure 2 can be compared directly to the figures shown in [1] (experimental “ $e_v \cdot p_i$ ”). The linear dependance in $\frac{P_{man}}{P_{amb}}$ is clear in the low and middle pressure ratio range (small throttle openings). As in [1], the slope of the lines is approximately 1.1 and varies with the level of acoustic resonance (as indicated by the values of “ $\frac{N}{\sqrt{T_{man}}}$ ”). At the end points however, for pressure ratios larger than 0.95, the volumetric efficiency lines curve up or down. Note that this region covers a large part of the operating range (medium to large throttle openings) despite the small change in pressure ratio. One possible explanation for the curving (which can also be observed for real engine data) is that the waves traveling back and forth in the intake manifold are partially reflected on the throttle plate; with varying throttle position, the level of reflection changes, and so do the conditions at which resonance occurs.

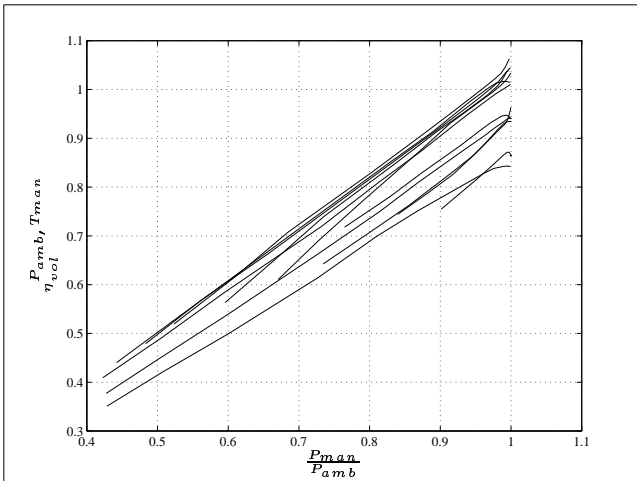


Figure 2: Simulated volumetric efficiency, $\eta_{vol}^{P_{amb}, T_{man}}$. Each line corresponds to a different value of $\frac{N}{\sqrt{T_{man}}}$ (from 106 to 403 in steps of 27).

4.2 Steady-state versus transient volumetric efficiency

In Figure 3, the simulated engine is run through a series of fast tip-ins and tip-outs (rise time of the throttle plate is 50 msec). The most important engine variables are plotted

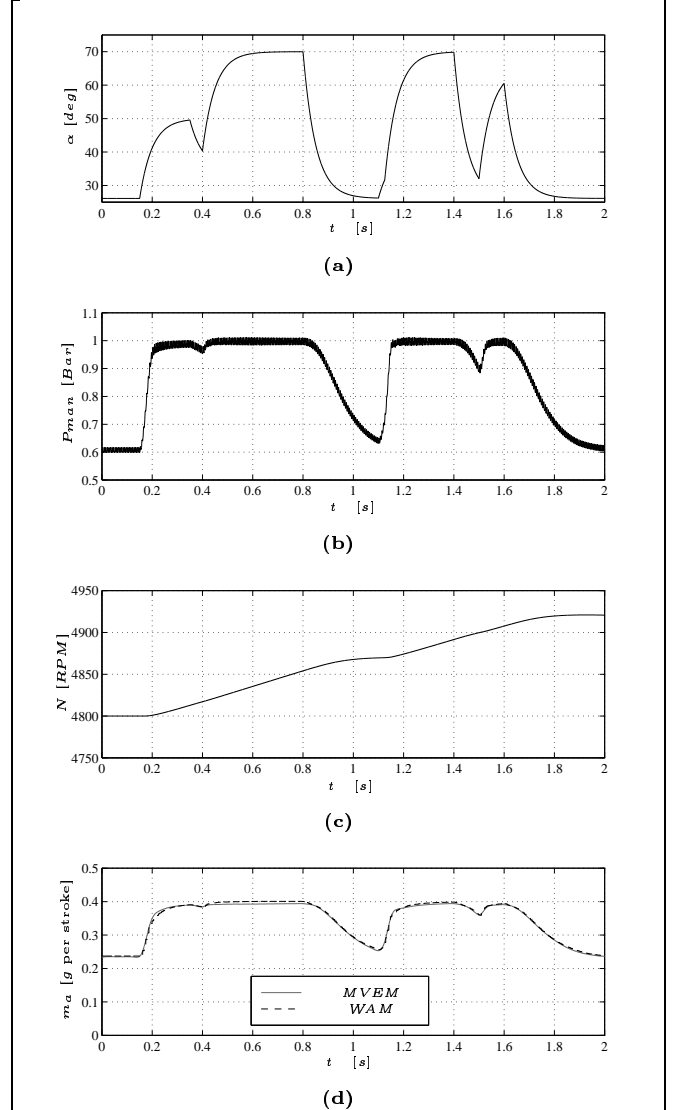


Figure 3: Testing the validity of steady-state volumetric efficiency maps during transient operation. Note that for the sake of convenience, air charge per stroke is compared instead of volumetric efficiency.

so that the operating range of the engine during the test can be judged. For each stroke, the induced air is recorded, and an equivalent mass flow rate is computed. This flow is compared to the one obtained using the speed density equation (21) (where the mean plenum pressure and temperature during the corresponding stroke are used as input to the speed density equation and to the steady-state volumetric efficiency map). As can be seen from the figure, despite the size and speed of the transient, the steady-state volumetric efficiency map gives error less than 2% in estimated cylinder air charge so that it can be concluded

that wave and inertial effects, heat transfer⁷ and backflow⁸ have only a limited impact on the accuracy of steady-state volumetric efficiency maps during transient operation.

4.3 Steady versus unsteady throttle air mass flow

In Appendix A, an improved steady flow model of the throttle air mass flow is given. In [1], this model was tested on a steady flow bench and was shown to describe the air flow with an excellent accuracy (error < 3% of actual flow) over the entire operating region. In an engine where the flow is typically unsteady, the model describes the *instantaneous* flow with the same accuracy, since the throttle body is much smaller than the wave length of the pumping fluctuations. However, for mean value engine modeling, it is the mean of the flow (over one event) which is of interest. In Figure 4, the mean of the throttle flow calculated with the wave action model (*WAM*) is compared to the mean value throttle model of Equation (33) in Appendix A.

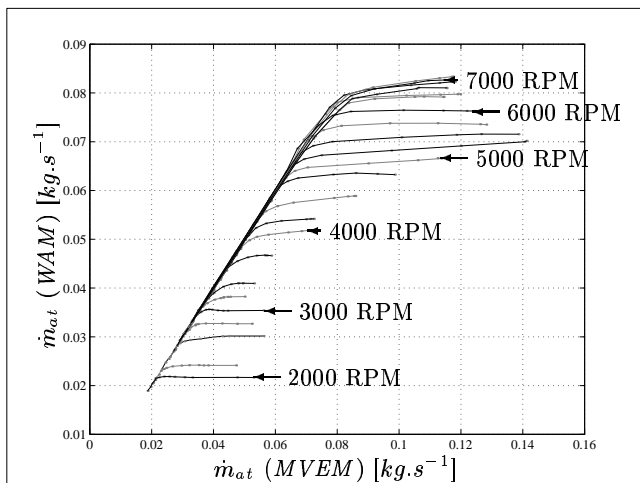


Figure 4: Comparison between the actual mean flow (simulated with the unsteady flow model, *WAM*) and the mean flow given by the *MVEM* of Equation (33). The isotachs⁹ vary from 2000 RPM to 7500 RPM in steps of 500 RPM. Above some throttle openings (depending on N), the isotachs flatten out indicating that the engine is no longer throttled by the butterfly valve but by the intake port instead. This figure should be compared with the experimental data of Figure 16(c) in Appendix A.

Despite the fact that both models are based on the same *instantaneous* flow model, large errors can be observed for large throttle openings (the regions where the isotachs⁹

⁷The cylinder-walls temperature was however kept constant throughout the simulation (both during steady-state mapping and during transient testing) so that the impact of varying cylinder-wall temperature during transient operation is not accounted for in these results.

⁸The variation in gas speciation in the runners due to the varying amount of backflow during transient is not accounted for in these results. However, simulations with simple in-cylinder models [24] suggest that this phenomenon is negligible.

⁹Lines connecting points of equal engine speed

flatten out in Figure 4). Since in the simulation, we have perfect knowledge of the background flow models, the off-diagonal points can only be explained as a result of the averaging process. This can be further clarified with the help of Figure 5.

Figure 5(b) shows the throttle flow model (with the throttle opened 80 deg.) which is used both in the *WAM* and in the *MVEM* models. Figure 5(a) shows the details of the pressure ratio, P_r across the throttle, during one engine cycle. The mean of the pressure ratio, $\overline{P_r}$, is also plotted. The pressure ratios (instantaneous and mean) are propagated through the throttle flow model of Figure 5(b) into Figure 5(c). The mean, $\overline{\dot{m}_{at}(P_r)}$ (over the cycle) of the instantaneous flow trace can then be compared with the *MVEM* value, $\dot{m}_{at}(\overline{P_r})$. For this particular case, the resulting error amounts to 49% of the actual mean flow rate.

The problem can be stated as follows: because of the strong nonlinearity of the throttle flow for P_r close to 1 (see Equation (38)), and because of the presence of pumping fluctuations in P_r , the mean of the \dot{m}_{at} function (Equation (33)) applied to (instantaneous) P_r can differ greatly from the \dot{m}_{at} function applied to the mean of P_r (in short: $\overline{\dot{m}_{at}(P_r)} \neq \dot{m}_{at}(\overline{P_r})$).

This phenomenon is typical of what happens with conventional mean value throttle models at large throttle openings (in Appendix A, modeling errors up to 60% are observed with real engine data, see Figure 16).

Obviously, this is a serious limitation of *MVEMs* close to *WOT*, especially in *AFR* control applications where accuracy over the entire operating range is of primary importance. Based on the analysis of Figure 5, it appears that an accurate mean value throttle model needs to depend not only on P_r and α , but also on the level of pumping fluctuations. Provided a measure of this level is available (a priori, in a MAP, or on line (measured/estimated)¹⁰), the revised model proposed in the section below can be used to improve the performance of *MVEMs*.

A revised mean value throttle model

For the sake of clarity and to avoid confusion, mean values (over one cycle) are “over-lined” ($\overline{(\quad)}$) in this section.

¹⁰In [25], an observer of the intake manifold pressure pumping fluctuations is proposed; however, for the current application, this observer would need some modifications so that it can be used as an estimator of the pumping fluctuations of P_r instead.

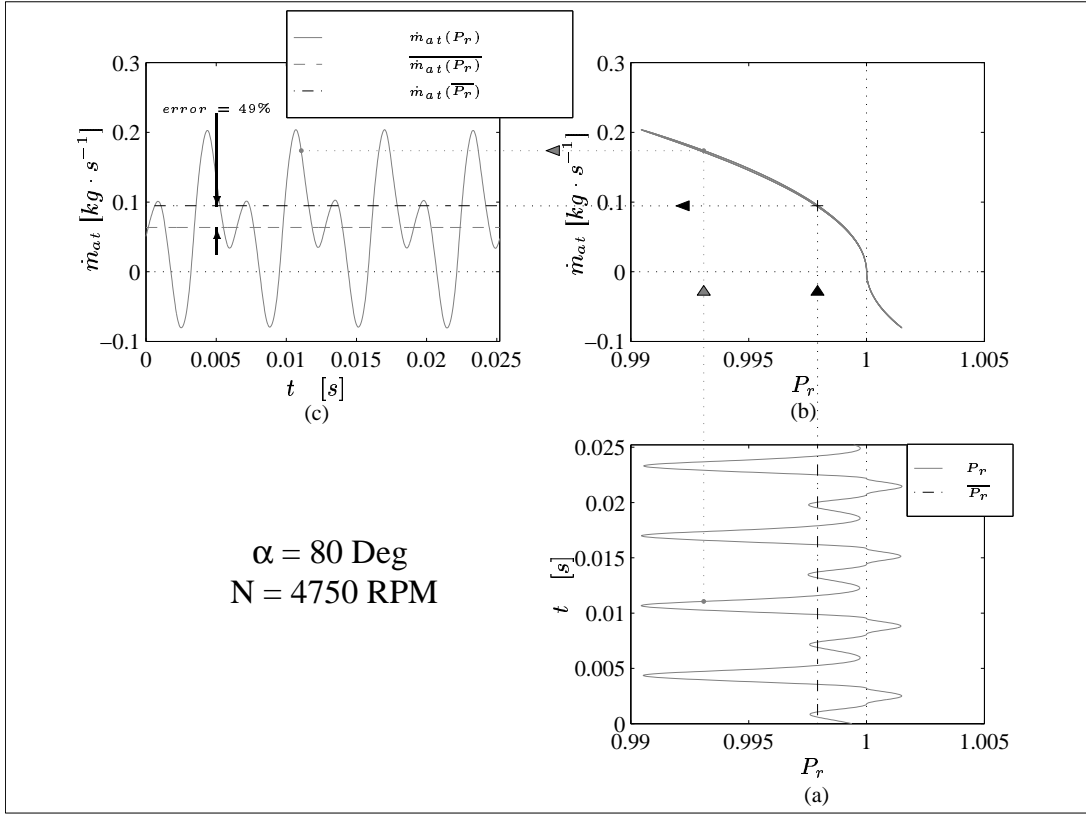


Figure 5: The effect of pumping fluctuations on the mean value throttle air mass flow model. \bar{x} denotes the mean of x .

By definition, the mean of the throttle air mass flow is

$$\begin{aligned}
 \overline{\dot{m}_{at}} &= \frac{P_{up}}{\sqrt{T_{amb}}} \beta_1(\alpha) \beta_2^*(P_r) \\
 &\approx \frac{\overline{P_{up}}}{\sqrt{T_{amb}}} \beta_1(\alpha) \overline{\beta_2^*(P_r)} \\
 &\neq \frac{\overline{P_{up}}}{\sqrt{T_{amb}}} \beta_1(\alpha) \beta_2^*(\overline{P_r}) \quad \text{Conventional mean value throttle model}
 \end{aligned} \quad (22)$$

where β_2^* and β_1 are defined in Appendix A. $P_r = \frac{P_{man}}{P_{up}}$ where P_{up} is the pressure upstream of the throttle plate.

Note that the approximation of $\overline{\beta_2^*(P_r)} = \beta_2^*(\overline{P_r})$ is the reason why conventional mean value throttle models fail close to *WOT*.

Alternatively, considering the fact that P_r is a periodic signal, it can be expanded in a Fourier series:

$$\begin{aligned}
 P_r(t) &= \overline{P_r(t)} + \Delta P_{r0} \sin(\omega_e t + \phi_0) \\
 &\quad + \Delta P_{r1} \sin(2\omega_e t + \phi_1) + \dots \quad (23)
 \end{aligned}$$

where ω_e is the engine event frequency (proportional to the engine speed). ΔP_{r0} and ΔP_{r1} are the amplitudes of the fundamental and the first harmonic components respectively. The ϕ 's represent the phasing of each components.

Ignoring the harmonics of rank 1 and above, P_r can be

approximated by P_{r0}

$$P_r(t) \approx P_{r0}(t) = \overline{P_r(t)} + \Delta P_{r0} \sin(\omega_e t + \phi_0) \quad (24)$$

Consequently $\overline{\beta_2^*(P_r)}$ can be approximated by $\beta_3(\overline{P_r}, \Delta P_{r0})$, where by definition

$$\begin{aligned}
 \beta_3(\overline{P_r}, \Delta P_{r0}) &= \overline{\beta_2^*(P_{r0})} \\
 &= \overline{\beta_2^*(\overline{P_r(t)} + \Delta P_{r0} \sin(\omega_e t))}
 \end{aligned} \quad (25)$$

β_3 is shown as a function of P_r in Figure 7, for various values of ΔP_{r0} . Note that β_3 is calculated directly from β_2^* and can therefore be mapped without any extra calibration.

Finally, the revised throttle model is given by

$$\begin{aligned}
 \overline{\dot{m}_{at}}(\alpha, P_{man}, P_{up}, T_{amb}, \Delta P_{r0}) &= \\
 &= \frac{P_{up}}{\sqrt{T_{amb}}} \beta_1(\alpha) \beta_3(\overline{P_r}, \Delta P_{r0}) \quad (26)
 \end{aligned}$$

The principle of the revised model is illustrated in Figure 6. For this particular case, the modeling error was decreased from 49% down to 11% of the actual mean flow rate.

In Figure 8, the data obtained with the *WAM* are used to compare the conventional mean value throttle model (Equation (33)) with the revised mean value throttle model

(Equation (26)). The maximum error is decreased from 65% down to 25%. Higher accuracy is in principle possible if P_r is approximated with a series of higher order. But the mapping complexity of β_3 increases exponentially with the order of the approximation.

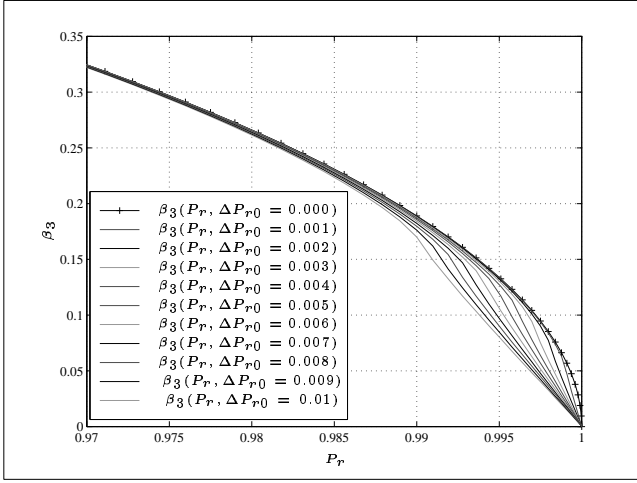


Figure 7: The revised β_3^* function: $\beta_3(P_r, \Delta P_{r0})$. The line marked with “+” ($\Delta P_{r0} = 0$) coincides with the β_3^* function.

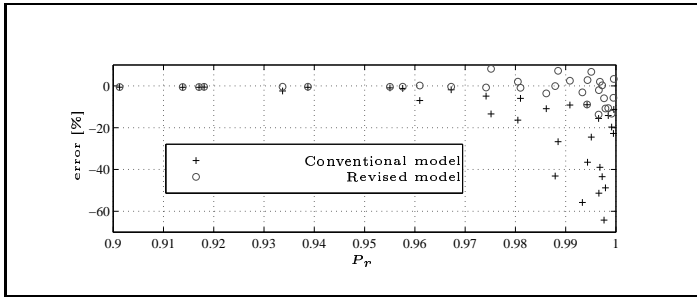


Figure 8: Comparison between conventional Mean Value Throttle Model and Revised Mean Value Throttle Model (including fundamental frequency of the pumping fluctuations).

4.4 Manifold filling state equations

It is common in *AFR* control to use a single-state differential equation (see Equation (27) below) to describe the time development of the manifold mean pressure. While this isothermal manifold model (referred to as *MVEM1* in the remainder of this paper) has proved very useful in many applications, it may require improvement in order to bring modern model-based *AFR* controllers to the level imposed by the new environmental regulations.

MVEM1:

$$\dot{P}_{man} = \frac{r T_{man}}{V_{man}} (\dot{m}_{at} - \dot{m}_{ap}) \quad (27)$$

In Figure 11, the single-state model is compared to unsteady flow simulation results. The engine is operated at constant speed and the throttle moved from 26.125 deg to

50 deg in 50 msec (rise time). As can be seen, the estimated mean pressure and mean throttle air mass flow are remarkably accurate. It is however interesting to notice that, despite these good results, the error in port air mass flow reaches 15% during transient.

In [5], one of the current authors discusses the fact that the isothermal assumption ($\dot{T}_{man} = 0$) which is normally used in the one-state manifold model may lead to a somewhat inaccurate description of the intake air density during tip-ins and tip-outs. It is suggested that mass conservation and energy conservation in the intake manifold should both be considered to properly describe the air dynamics. This two-state mean value model (referred to as *MVEM2* in the remainder of this paper) is given in Equation (28).

MVEM2:

$$\begin{aligned} \dot{P}_{man} &= P_{man} \frac{\gamma r T_{amb}}{V_{man} P_{man}} \\ &\quad \left(\dot{m}_{at} - \frac{T_{man}}{T_{amb}} \dot{m}_{ap} + \frac{\gamma - 1}{\gamma r} \frac{\dot{Q}_{ext}}{T_{amb}} \right) \\ \dot{T}_{man} &= T_{man} \frac{\gamma r T_{amb}}{V_{man} P_{man}} \\ &\quad \left(\dot{m}_{at} \left(1 - \frac{1}{\gamma} \frac{T_{man}}{T_{amb}} \right) - \frac{T_{man}}{T_{amb}} \dot{m}_{ap} \left(1 - \frac{1}{\gamma} \right) \right. \\ &\quad \left. + \frac{\gamma - 1}{\gamma r} \frac{\dot{Q}_{ext}}{T_{amb}} \right) \end{aligned} \quad (28)$$

For the sake of completeness, heat transfer has been included in the model.

$$\dot{Q}_{ext} = h (T_{amb} - T_{man}) \quad (29)$$

Again, this model is tested against the *WAM*. Some results are shown in Figure 12 for the case of no heat transfer ($h = 0$, i.e. adiabatic *MVEM2*). The improvement in the port air mass flow estimate is clear, and there is no doubt that the two-state model is better suited for transient port air mass flow estimation. Note however that the estimated temperature excursions are too large, which explains partially the remaining error on \dot{m}_{ap} .

In Figure 13, the heat transfer coefficient, h , is adjusted so that the Two-State Mean Value Engine Model (*MVEM2*) model fits the plenum temperature trace optimally. This was achieved with a value of $25 \text{ W} \cdot \text{K}^{-1}$. The accuracy of the estimated port air mass flow is good.

4.5 Pressure losses between plenum and intake runners

As an attempt to further improve the temperature and port air mass flow estimates, the Four-state *MVEM* of Equation (30) is proposed. As can be seen in Figure 9, the intake manifold is now modeled as two capacitances in series (one for the plenum and one for all 4 intake runners) separated by a resistive flow element. Energy and mass

conservation is applied in both volumes (including heat transfer) and the flow through the junction is modeled as an isentropic converging nozzle discharging into a sudden enlargement. The resulting 4-state model is referred to as *MVEM₄* in the remainder of this paper. P_m and T_m are the pressure and temperature in the manifold plenum (volume V_m), P_p and T_p are the pressure and temperature in the intake pipes (volume V_p).

MVEM₄:

$$\begin{aligned}
\dot{P}_m &= P_m \frac{\gamma r T_{amb}}{V_m P_m} \\
&\quad \left(\dot{m}_{at} - \frac{T_m}{T_{amb}} \dot{m}_{aj} + \frac{\gamma - 1}{\gamma r} \frac{\dot{Q}_m}{T_{amb}} \right) \\
\dot{T}_m &= T_m \frac{\gamma r T_{amb}}{V_m P_m} \\
&\quad \left(\dot{m}_{at} \left(1 - \frac{1}{\gamma} \frac{T_m}{T_{amb}} \right) - \frac{T_m}{T_{amb}} \dot{m}_{aj} \left(1 - \frac{1}{\gamma} \right) \right. \\
&\quad \left. + \frac{\gamma - 1}{\gamma r} \frac{\dot{Q}_m}{T_{amb}} \right) \\
\dot{P}_p &= P_p \frac{\gamma r T_m}{V_p P_p} \\
&\quad \left(\dot{m}_{aj} - \frac{T_p}{T_m} \dot{m}_{ap} + \frac{\gamma - 1}{\gamma r} \frac{\dot{Q}_p}{T_m} \right) \\
\dot{T}_p &= T_p \frac{\gamma r T_m}{V_p P_p} \\
&\quad \left(\dot{m}_{aj} \left(1 - \frac{1}{\gamma} \frac{T_p}{T_m} \right) - \frac{T_p}{T_m} \dot{m}_{ap} \left(1 - \frac{1}{\gamma} \right) \right. \\
&\quad \left. + \frac{\gamma - 1}{\gamma r} \frac{\dot{Q}_p}{T_m} \right)
\end{aligned} \tag{30}$$

where

$$\begin{aligned}
\dot{Q}_m &= h_m (T_{amb} - T_m) \\
\dot{Q}_p &= h_p (T_{amb} - T_p)
\end{aligned} \tag{31}$$

are the heat transfers in the plenum and in the runners respectively and where

$$\dot{m}_{aj} = K_{aj} \frac{P_m}{\sqrt{T_m}} \sqrt{\left(\frac{P_p}{P_m} \right)^{\frac{2}{\gamma}} - \left(\frac{P_p}{P_m} \right)^{\frac{\gamma+1}{\gamma}}} \tag{32}$$

represents the flow between the plenum and the runners. K_{aj} plays the role of a resistance flow coefficient.

As can be seen in Figure 14, both temperatures, in the plenum and in the runners, are estimated with a good accuracy. As a direct consequence, the port air mass flow accuracy is also improved and the error never exceeds 3%. These results were obtained with no heat transfer in the *MVEM₄* model (adiabatic assumption). However, analysis of the eigenfrequencies of the Four-state model shows that the model is extremely stiff and that it may be unpractical for real applications.

4.6 Experimental results

Unlike the other figures, Figure 10 shows experimental data taken from a real engine (displacement volume: 1.3 l; intake manifold volume: 4.3 l); the transient temperature excursions can clearly be observed during tip-in and tip-out. In order to obtain these measurements, a fast 0.4 mm Nickel/Chromium-Nickel/Aluminium type K thermocouple with a time constant of 200 ms was mounted in the intake plenum. By “inverting” (using Kalman filtering) the air dynamics described by the Two-state model, it was possible to reconstruct the actual manifold temperature and deviations up to 18 K were estimated. A heat transfer coefficient of $20 \text{ W} \cdot \text{K}^{-1}$ was found to give the best results (in terms of estimated manifold pressure, estimated throttle air mass flow and estimated measured manifold temperature).

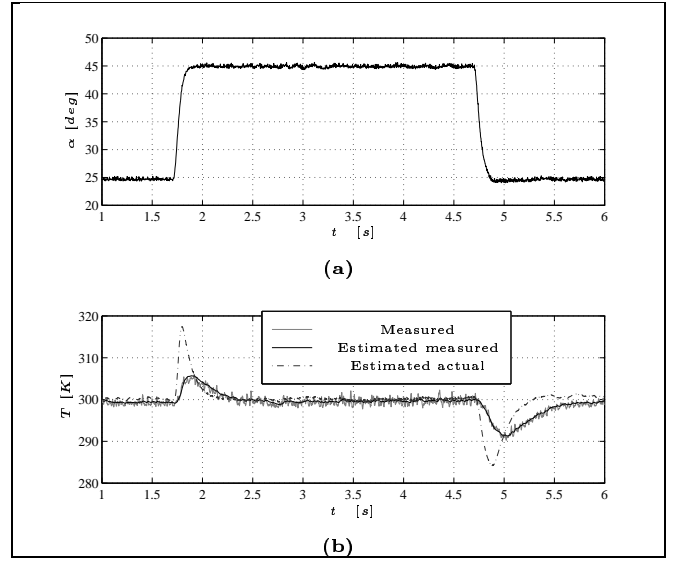


Figure 10: Measured and estimated transient temperature excursions. Adapted from [25].

5 CONCLUSIONS

The validity of Mean Value Engine Modeling during transient operation has been studied. Because *MVEM*'s are mainly intended for *AFR* control applications, the models are evaluated on the basis of the accuracy of the estimated port air mass flow. Unfortunately, non-intrusive measurement of the port air mass flow is impossible¹¹; the approach followed in this paper, is therefore to compare mean value models (as a whole as well as in detail) to a model of higher complexity (*1D* solution of homentropic unsteady flows). The conclusions drawn from this work are therefore purely theoretical and still need to be confirmed through experiments.

¹¹In [24], a new type of intake port air mass flow sensor is presented. This sensor is however not completely non-intrusive as it may have an impact on the acoustic phenomena of the intake manifold.

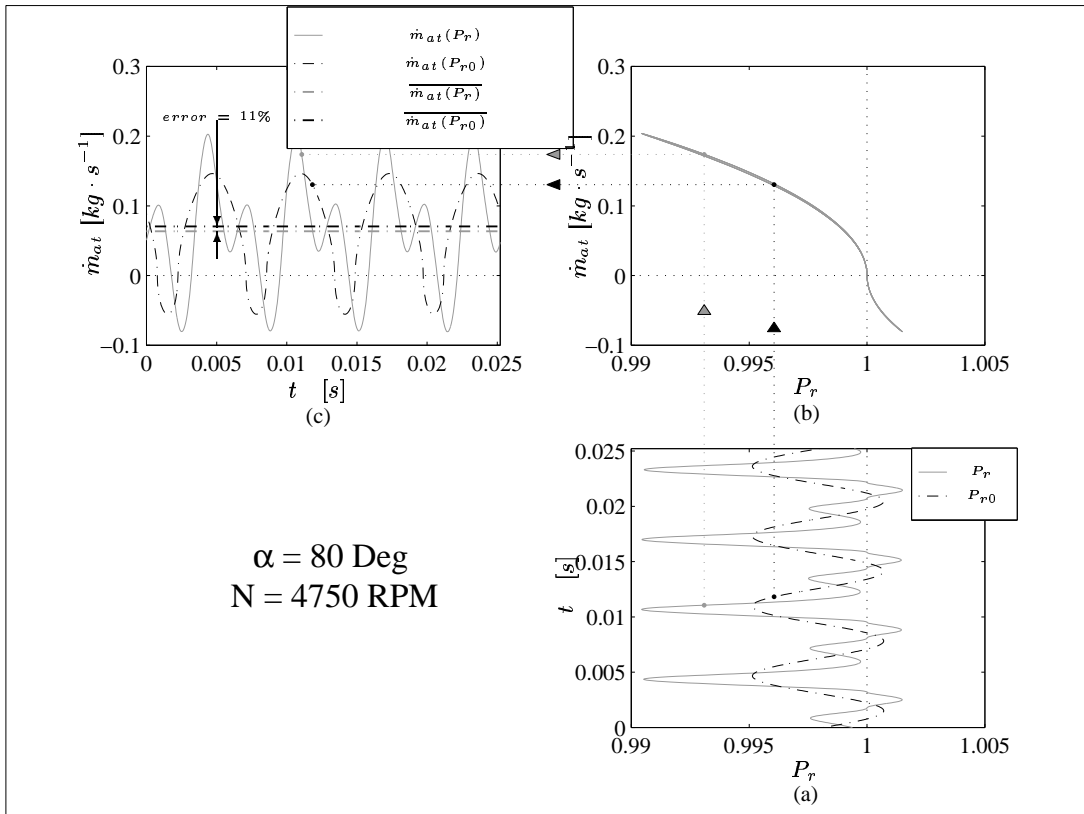


Figure 6: Modus operandi of the Revised Mean Value Throttle air mass flow Model, including the effects of pumping fluctuations. Note how P_r is approximated by P_{r0} (a), and how $\dot{m}_{at}(P_r)$ gets approximated by $\dot{m}_{at}(P_{r0})$ (c).

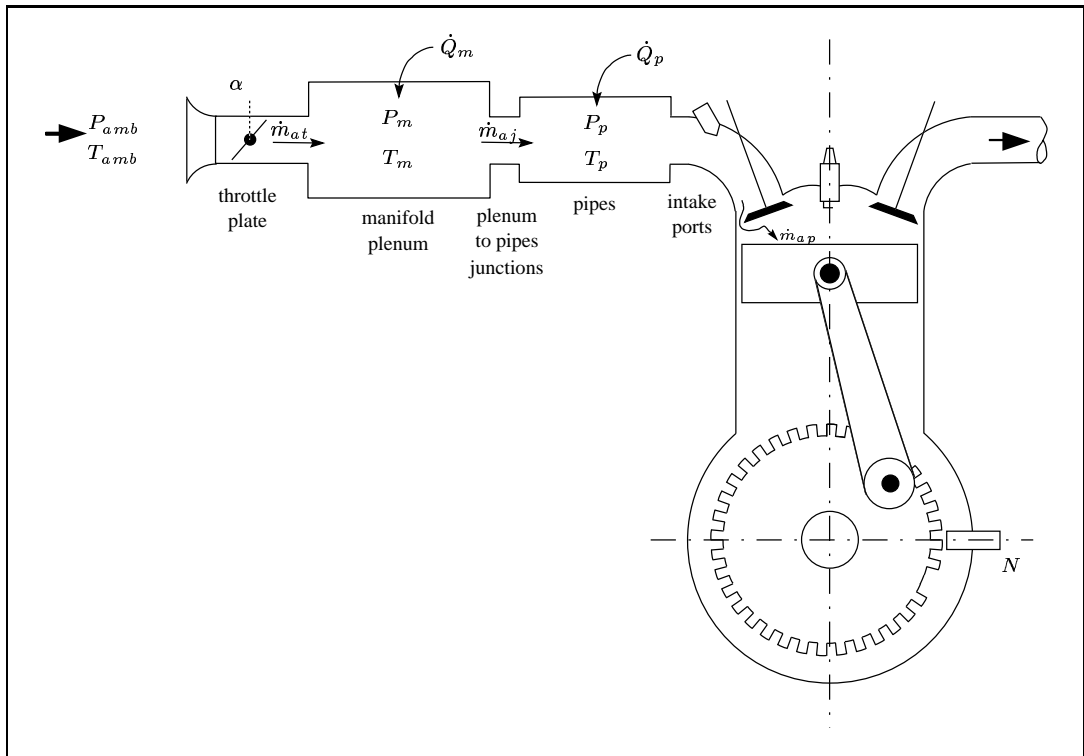


Figure 9: 4-state modeling of the intake manifold dynamics ($MVEM_4$).

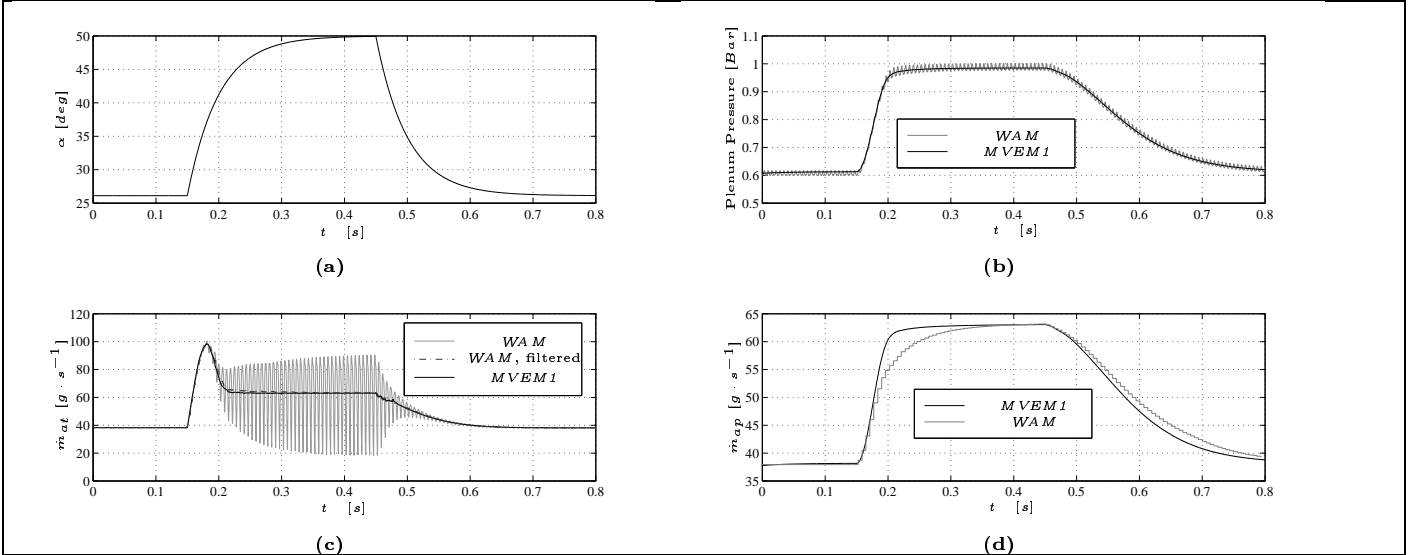


Figure 11: Testing the validity of the single-state *MVEM1*. The port air mass flow, \dot{m}_{ap} is largely underestimated during tip-in and over-estimated during tip-out even though manifold pressure, P_{man} , and throttle air mass flow, \dot{m}_{at} , are estimated with a remarkable accuracy.

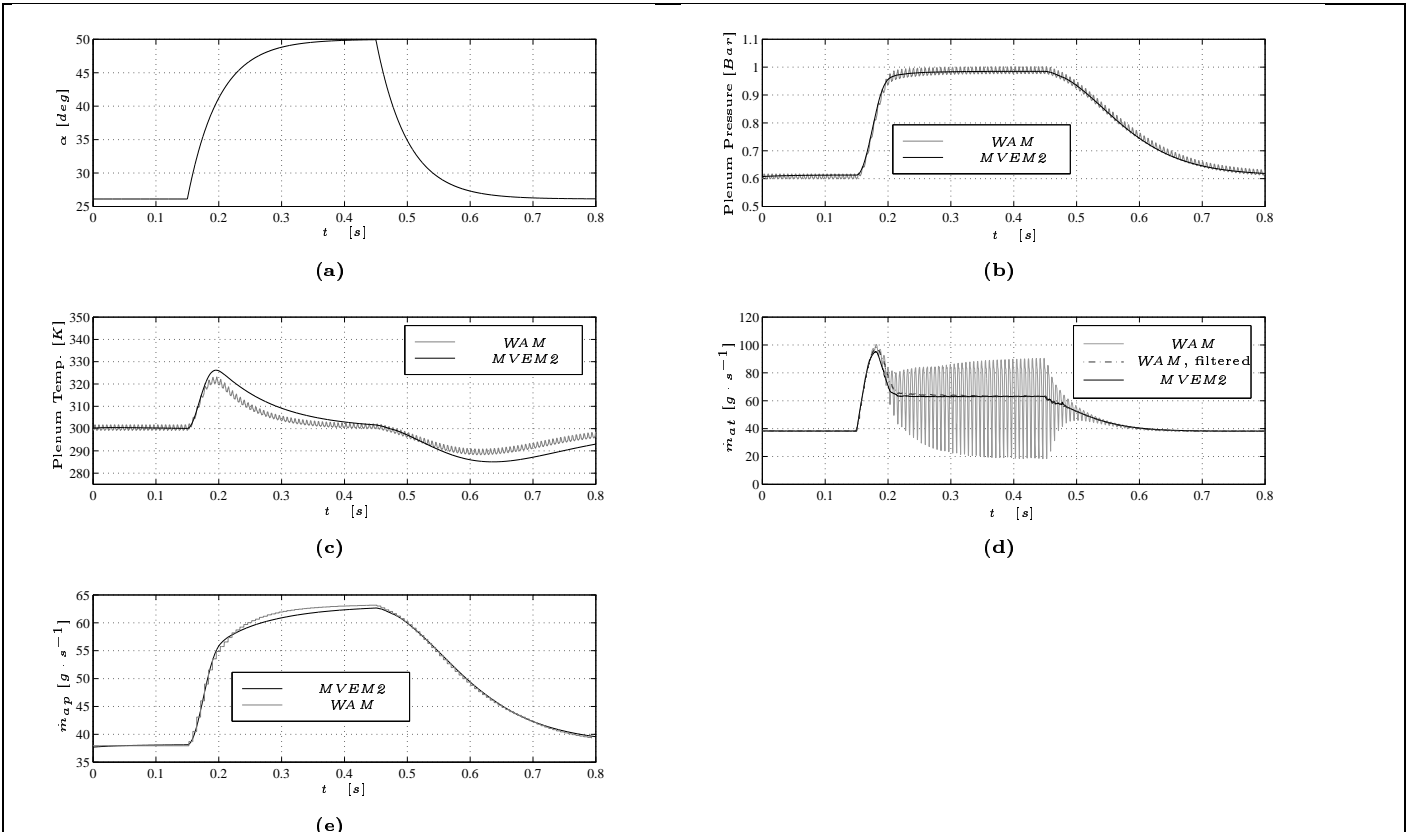


Figure 12: Testing the validity of the adiabatic Two-state *MVEM2*. The heat transfer coefficient, h is set to zero in this version of the *MVEM2* (but not in the *WAM*).

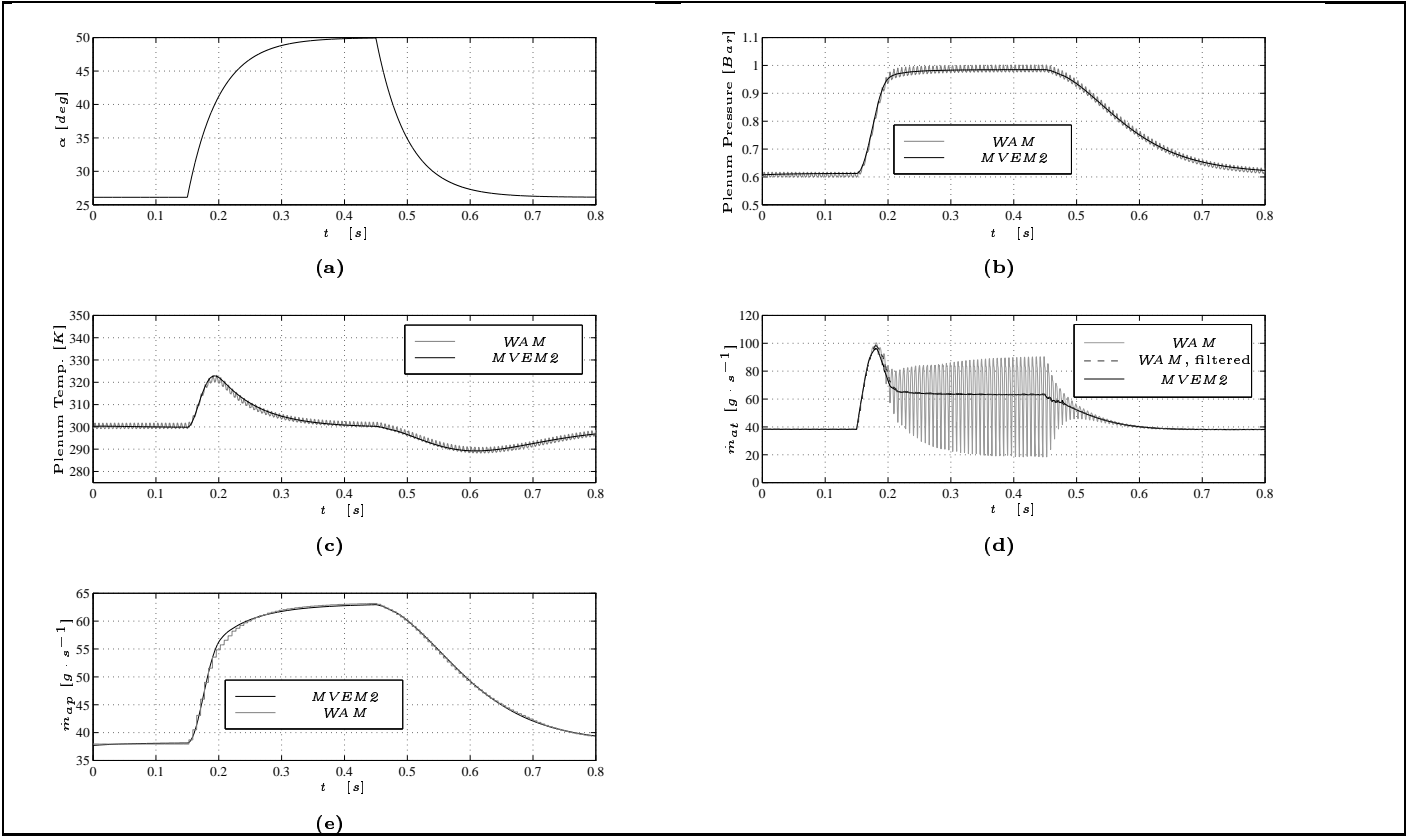


Figure 13: Testing the validity of the Two-state $MVEM2$, including heat transfer ($h = 25 \text{ W} \cdot \text{K}^{-1}$).

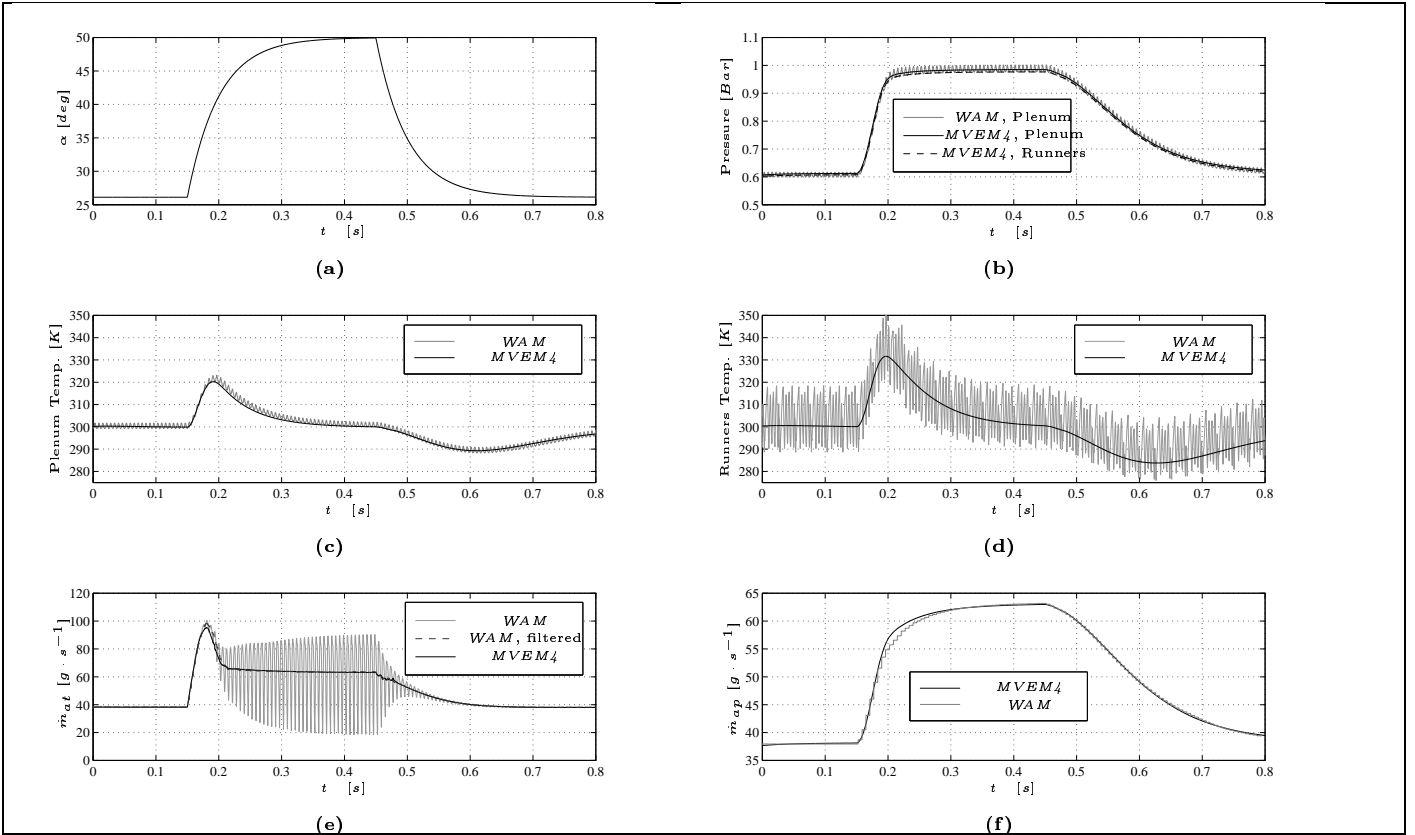


Figure 14: Testing the validity of the Four-state $MVEM4$. Note that the temperature of the runners shown in Figure 14(d) was “measured” (simulated) at the half way point between the plenum and the intake port. Heat transfer was set to zero in the $MVEM4$ (in the plenum and in the runners, $h_m = h_p = 0$).

These results can be summarized in four points:

1. Despite the complex nature of acoustic phenomena during transients (rapid throttle opening/closing, varying load on the crank), conventional steady-state volumetric efficiency maps are capable of describing the engine breathing performance with a remarkable accuracy also during fast transient operation; consequently, the so-called speed density equation (see Equations (2) or (4)) provides a very accurate description of the port air mass flow, provided the mean air density is known with equivalent accuracy in the intake manifold. However, the effect of varying cylinder-wall temperature during transient operation still needs to be investigated.
2. Because of the strong nonlinearity of the throttle air mass flow model for pressure ratios close to unity, the isentropic converging nozzle/sudden enlargement model becomes very inaccurate close to *WOT*. However, provided the level of pumping fluctuations on the pressure ratio signal is known, this accuracy can be brought back to an acceptable level.
3. The isothermal assumption ($\dot{T}_{man} = 0$) which is normally used in the one-state manifold model leads to a somewhat inaccurate description of the intake air density during tip-ins and tip-outs. Mass conservation and energy conservation in the intake manifold should both be considered in order to properly describe the air dynamics. The difference between the isothermal single-state model and the two-state model can be of up to 15% in port air mass flow¹². The importance of heat transfer was also demonstrated and a value for the heat transfer coefficient was proposed. Experiments conducted on an engine confirm the temperature excursions during fast transients.
4. The accuracy of the two-state *MVEM* model can be slightly improved if the friction losses between the plenum and the intake runners are included. However, the resulting four-state model may be too stiff for most practical applications and the small gain in accuracy might not be worth the increased model complexity.

REFERENCES

- [1] E. Hendricks, M. Jensen, A. Chevalier, S. C. Sorenson, D. Trumphy, and J. Asik, "Modelling of the Intake Manifold Filling Dynamics," *SAE Technical Paper*, no. 960037, 1996.
- [2] D. Broome, "Induction Ram, Part Two: Inertial Aspects of Induction Ram," *Automobile Engineer*, pp. 180–184, May 1969.
- [3] D. Broome, "Induction Ram, Part Three: Wave Phenomena and the Design of Ram Intake Systems," *Automobile Engineer*, pp. 262–267, June 1969.
- [4] L. A. Smith, T. Fickenscher, and R. P. Osborne, "Engine Breathing - Steady Speed Volumetric Efficiency and its Validity Under Transient Engine Operation," *SAE Technical Paper*, no. 1999-01-0212, 1999.
- [5] M. Müller, "Mean Value Modelling of Turbocharged Spark Ignition Engines," Master's thesis, The Technical University of Denmark, Institute of Automation and Department of Energy, 1997.
- [6] R. Benson, R. Garg, and D. Woollatt, "A Numerical Solution of Unsteady Flow Problems," *International Journal of Mechanical Science*, vol. 6, pp. 117–144, 1964.
- [7] R. Benson, "Numerical Solution of One-Dimensional Non-Steady Flow with Supersonic and Subsonic Flows And Heat Transfer," *International Journal of Mechanical Science*, vol. 14, pp. 635–642, 1972.
- [8] R.S. Benson, ed., *The Thermodynamics and Gas Dynamics of Internal Combustion Engines, Volume 1*. Oxford University Press, 1982. Walton Street, Oxford OX2 6DP, UK.
- [9] M. Poloni, D. Winterbone, and J. Nichols, "Comparison of Unsteady flow Calculations in a Pipe by the Method of Characteristics and the Two-Step Differential Lax-Wendroff Method," *International Journal of Mechanical Science*, vol. 29, pp. 367–378, 1987.
- [10] P. Lax and B. Wendroff, "Systems of Conservation Laws," *Communications of Pure and Applied Mathematics*, vol. 13, pp. 217–237, 1960.
- [11] T. Bulaty and H. Niessner, "Calculation of 1-D Unsteady Flows in Pipe Systems of I.C. Engines," *Journal of Fluids Engineering*, vol. 107, pp. 407–412, 1985.
- [12] A. Shapiro, *The Dynamics and Thermodynamics of Compressible Fluid Flow*, vol. 1. The Ronald Press Company, New York, 1954.
- [13] L. Moody, "Friction Factors for Pipe Flow," *Transactions of the ASME*, vol. 8, pp. 671–684, 1944.
- [14] G. Blair and J. Goulburn, "The Pressure-Time History in the Exhaust System of a High-Speed Reciprocating Internal Combustion Engine Study," *SAE Technical Paper*, no. 670477, 1967.
- [15] J. Pichard, "Mécanique des Fluides Appliquée aux Moteurs a Capsulisme," *Techniques de l'Ingénieur*, Mar. 1973. In french.
- [16] H. Daneshyar, "Numerical Solution of Gas Flow Through an Engine Cylinder," *International Journal of Mechanical Science*, vol. 10, pp. 711–722, 1968.

¹²However, for manifold volumes small compared to the engine displacement volume (and/or for slow throttle transients), the temperature excursions are small, and the isothermal single-state model is still suitable.

- [17] A. Bicen, C. Vafidis, and J. Whitelaw, "Steady and Unsteady Airflow Through the Intake Valve of a Reciprocating Engine," *Journal of Fluids Engineering*, vol. 107, pp. 413–420, Sept. 1985.
- [18] G. Woschmi, "Universally Applicable Equation for the Instantaneous Heat Transfer Coefficient in the Internal Combustion Engine," *SAE Technical Paper*, no. 670931, 1967.
- [19] J. Bingham and G. Blair, "An Improved Branched Pipe Model for Multi-Cylinder Automotive Engine Calculations," *Proceedings from the Institution of Mechanical Engineers*, vol. 199, no. D1, pp. 65–77, 1985.
- [20] G. Blair, "Non-Isentropic Analysis of Branched Flow in Engine Ducting," *SAE Technical Paper*, no. 940395, 1994.
- [21] R. Benson, P. Baruah, and R. Sierens, "Steady and Non-Steady Flow in a Simple Carburettor," *Proceedings from the Institution of Mechanical Engineers*, vol. 188, pp. 537–548, 1974.
- [22] G. Blair and M. Johnston, "Unsteady Flow Effects in Exhaust Systems of Naturally Aspirated, Crankcase Compression Two-Cycle Internal Combustion Engines," *SAE Technical Paper*, no. 680594, 1968.
- [23] E. Buckingham, "On Physically Similar Systems; Illustration of the Use of Dimensional Equations," *The Physical Review (American Physical Society)*, vol. IV (Second Series), no. 4, pp. 345–376, 1914.
- [24] M. Føns, "Indførelse af Recirkulering af Udstødningsgas (EGR) i SI-Motorer," Master's thesis, The Technical University of Denmark, Department of Energy and Institute of Automation, 1997. In danish.
- [25] A. Chevalier and C. W. Vigild, "Predicting the Port Air Mass Flow of SI Engines in A/F Ratio Control Applications," *SAE Technical Paper*, no. To be published, 2000.

ACRONYMS

1D One-Dimensional

ABDC .. After Bottom Dead Center

AFR Air/Fuel Ratio

ATDC .. After Top Dead Center

BBDC .. Before Bottom Dead Center

BTDC .. Before Top Dead Center

DTU Technical University of Denmark

EVO Exhaust Valve Opening

FDM Finite Difference Methods

IC Internal Combustion

IVC Intake Valve Closing

LW2 Two-Step Lax-Wendroff

MAF Mass Air Flow

MMOC Mesh Method of Characteristics

MPI Multi-Point Injection

MVEM Mean Value Engine Model

MVEM1 Single-State Mean Value Engine Model

MVEM2 Two-State Mean Value Engine Model

MVEM4 Four-State Mean Value Engine Model

N&S Navier and Stoke

RPM Revolutions Per Minute

SAE Society for Automotive Engineers

SI Spark Ignition

WAM Wave Action Model

WOT Wide Open Throttle

VARIABLES

A Pipe section area, [m^2]

α Throttle plate angle (position), [$deg.$]

β_1 Discharge coefficient at the throttle plate

β_2 Compressibility coefficient at the throttle plate (1-channel model)

β_2^* Compressibility coefficient at the throttle plate (2-channel model)

β_3 Compressibility coefficient at the throttle plate (including pumping fluctuations)

C Vector function of *W* (*LW2*)

c Local speed of sound, [$m \cdot s^{-1}$]

ΔP_{r0} Amplitude of the fundamental component of P_r

ΔP_{r1} Amplitude of the 1st harmonic of P_r

Δt Time step in the mesh grid, [s]

Δx Mesh grid size, [m]

\dot{m}_a Air mass flow rate, [$kg \cdot s^{-1}$]

\dot{m}_{aj} Air mass flow rate at the junction between plenum and runners, [$kg \cdot s^{-1}$]

\dot{m}_{ap} Port air mass flow rate, [$kg \cdot s^{-1}$]

\dot{m}_{at} Throttle air mass flow rate, [$kg \cdot s^{-1}$]

\dot{q} Convective heat transfer, [$j \cdot s^{-1} \cdot kg^{-1}$]
 \dot{Q}_m Rate of heat transfer in the plenum, [$j \cdot s^{-1}$]
 \dot{Q}_p Rate of heat transfer in the pipes, [$j \cdot s^{-1}$]
 η_{vol}^{amb} Volumetric efficiency based on ambient conditions
 $\eta_{vol}^{P_{amb}, T_{man}}$ Volumetric efficiency based on barometric pressure, P_{amb} , and intake manifold temperature, T_{man}
 η_{vol}^{man} Volumetric efficiency based on intake manifold conditions
 F Vector function of W (*LW2*)
 h_0 Stagnation enthalpy, [$j \cdot kg^{-1}$]
 λ Normalized air/fuel ratio
 m_a Mass of fresh air trapped in a cylinder, [kg]
 M_{down} Mach number downstream the throttle plate
 N Engine speed, [RPM]
 P Local pressure, [Pa]
 P_{amb} Atmospheric manifold pressure, [Pa]
 P_D Throat pressure in dominant channel (throttle plate model), [Pa]
 P_{exh} Exhaust pressure, [Pa]
 P_m Mean plenum pressure, [Pa]
 P_{man} Mean intake manifold pressure, [Pa]
 P_p Mean pipe pressure, [Pa]
 P_r Pressure ratio
 P_{r0} Approximation of P_r , including fundamental frequency
 P_S Throat pressure in residual channel (throttle plate model), [Pa]
 P_{up} Pressure upstream the throttle plate, [Pa]
 ρ Local density, [$kg \cdot m^{-3}$]
 ρ_{up} Density upstream the throttle plate, [$kg \cdot m^{-3}$]
 t Time, [s]
 T_{amb} Atmospheric manifold temperature, [K]
 T_m Mean plenum temperature, [K]
 T_{man} Mean intake manifold temperature, [K]
 T_p Mean pipe temperature, [K]
 T_{up} Temperature upstream the throttle plate, [K]

T_w Local pipe wall temperature, [K]
 u Local velocity, [$m \cdot s^{-1}$]
 u_{up} Velocity upstream the throttle plate, [$m \cdot s^{-1}$]
 W Vector of dependent variables (*LW2*)
 ω_e Engine event frequency, [$rad \cdot s^{-1}$]
 x pipe abscissa

CONSTANTS

$b_{10} \dots b_{13}$ Fitting constant for the throttle air mass flow model
 c_p Specific heat of air at constant pressure, 1004.5 $j \cdot kg^{-1} \cdot K^{-1}$
 D Local pipe diameter, [m]
 δ Fitting constant for the throttle air mass flow model
 f Pipe friction factor
 f_t Pressure drop coefficient of throttle plate
 γ = $\frac{c_p}{c_v}$ Ratio of specific heats, 1.40 for air
 h Heat transfer coefficient [$j \cdot s^{-1} \cdot K^{-1}$]
 h_m Heat transfer coefficient in plenum, [$j \cdot s^{-1} \cdot K^{-1}$]
 h_p Heat transfer coefficient in pipe, [$j \cdot s^{-1} \cdot K^{-1}$]
 K_{aj} Throttle plate flow coefficient
 ν Fitting constant for the throttle air mass flow model
 P_{rc} Critical pressure ratio (at which a throat becomes sonic)
 r Specific gas constant, 287.0 $j \cdot kg^{-1} \cdot K^{-1}$ for air
 V_{disp} Engine displacement, [m^3]
 V_m Plenum volume [m^3]
 V_{man} Intake manifold volume, [m^3]
 V_p Total pipe volume [m^3]

OPERATORS

\bar{x} Mean of x

A Steady-state modeling of the flow across a butterfly valve

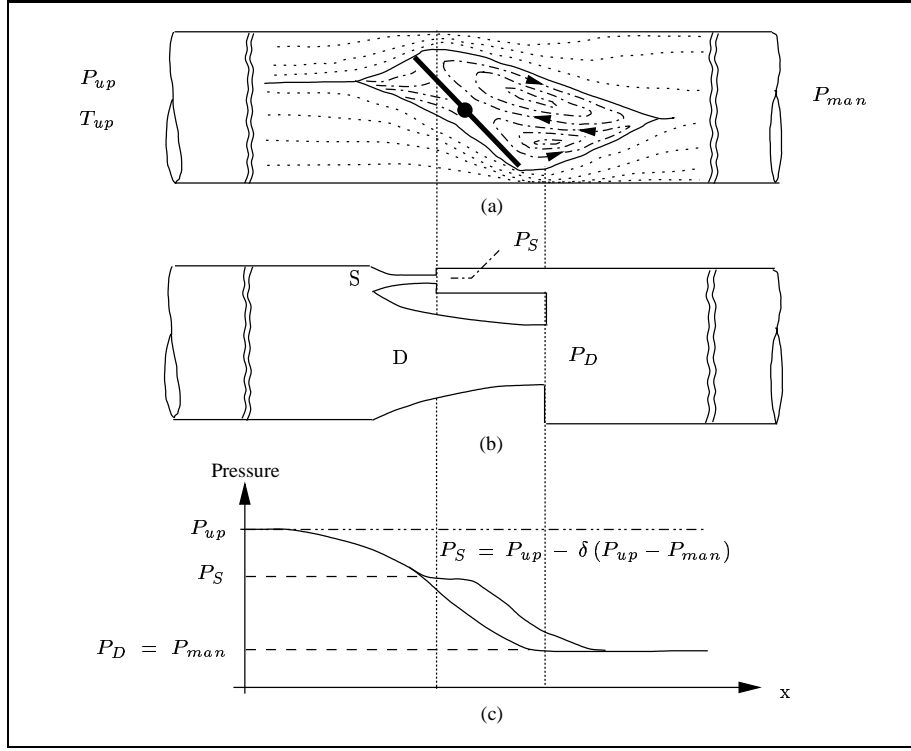


Figure 15: A 2-channel throttle air mass flow model. It is obvious from basic geometric considerations and flow visualization studies that all the air expands through two converging nozzles and then separates into two jet flows and one central eddy region (figure (a)). It is therefore more realistic to treat the throttle plate as two physically separated parallel flow fields: a dominant flow (large flow rate, region D in figure (b)) between the converging throttle plate and the wall, and a residual flow (small flow rate, region S in figure (b)) between the abrupt edge of the throttle plate and the wall. A sketch of the pressure along the two flows is given in figure (c). Clearly, both flows are seeing the same upstream stagnation conditions (assumed to be equal to the upstream conditions P_{up} , T_{up}). However, the separation of the flow in the accelerating region combined with a residual flow throat positioned upstream the dominant flow throat, leads to different throat pressures (the residual throat pressure P_S being always higher than the dominant throat pressure P_D). Like in the conventional one-channel model, the pressure is assumed constant downstream the throttle and $P_D = P_{man}$, where P_{man} is the (downstream) manifold pressure. δ is a fitting constant.

The isentropic converging nozzle/sudden enlargement model which is normally used to describe the throttle air mass flow is far too inaccurate. Because the flow splits along two paths across the plate (one large dominant flow (D), and one small residual flow (S), see Figure 15), a more accurate two-channel model is proposed in [1]. This model is made up of two isentropic converging nozzle/sudden enlargement models in parallel. In the dominant channel, the pressure loss at the throat amounts to the total pressure loss across the throttle ($P_{up} - P_{man}$), whereas, in the residual channel, the pressure loss only amounts to a part, δ ($\delta \in [0, 1]$) of the total pressure loss ($\delta(P_{up} - P_{man})$). Finally, the contribution of the residual flow is ν times that of the dominant flow, where ν is a fitting constant. The model is summarized below:

$$\dot{m}_{at}(\alpha, P_{man}, P_{up}, T_{amb}) = \frac{P_{up}}{\sqrt{T_{amb}}} \beta_1(\alpha) \beta_2^*(P_r) \quad (33)$$

where

$$\beta_2^*(P_r) = \frac{1}{\nu + 1} \beta_2(P_r) + \frac{\nu}{\nu + 1} \beta_2(1 - \delta(1 - P_r)) \quad (34)$$

where

$$P_r = \frac{P_{man}}{P_{up}} \quad (35)$$

where

$$\beta_2(x) = \frac{\sqrt{\max(x, P_{rc})^{\frac{1}{\gamma}} - \max(x, P_{rc})^{\frac{\gamma+1}{\gamma}}}}{\sqrt{P_{rc}^{\frac{1}{\gamma}} - P_{rc}^{\frac{\gamma+1}{\gamma}}}} \quad (36)$$

$$P_{rc} = \left(\frac{2}{\gamma+1}\right)^{\frac{\gamma}{\gamma-1}} \approx 0.5283$$

and where

$$\beta_1(\alpha) = b_{10} + b_{11} \cos(\alpha) + b_{12} \cos^2(\alpha) + b_{13} \cos^3(\alpha) \quad (37)$$

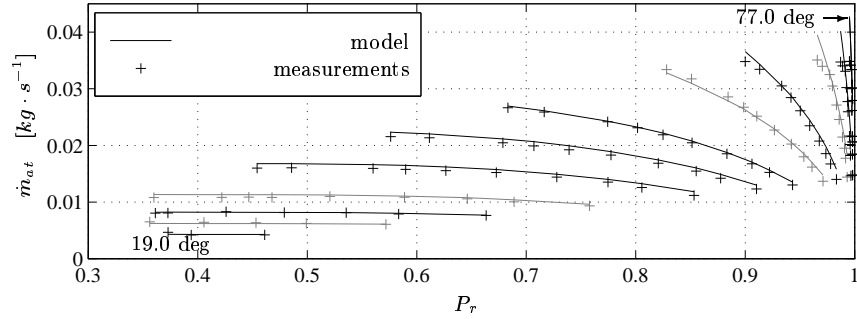
P_r is the pressure ratio across the throttle plate. P_{rc} is the pressure ratio threshold below which the flow is sonic at a throat. β_2 , β_2^* and β_1 are functions which account for compressibility and throat area changes. δ , ν and $b_{10} \dots b_{13}$ are fitting constants.

For pressure ratios above 0.9, the flow becomes extremely sensitive to pressure ratio variations:

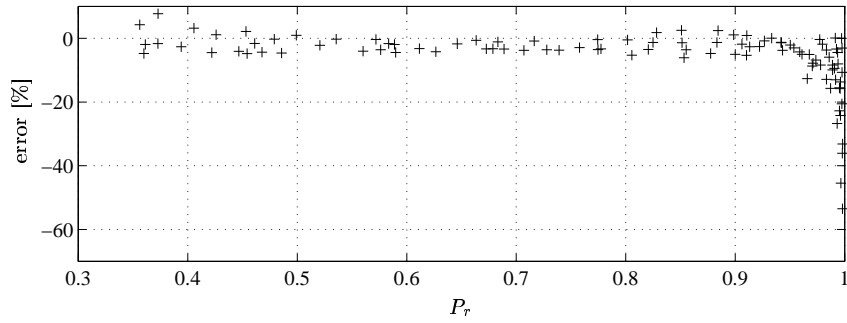
$$\lim_{P_r \rightarrow 1} \frac{\partial \dot{m}_{at}}{\partial P_r} = -\infty \quad (38)$$

and it is therefore important to know accurately not only the pressure downstream the throttle, P_{man} , but also the pressure upstream, P_{up} .

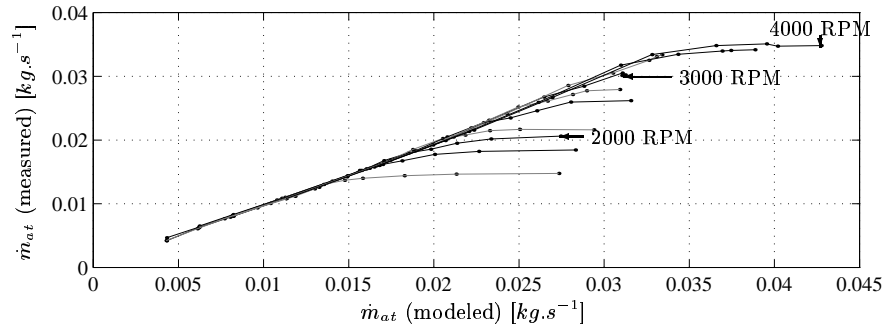
In Figure 16, the accuracy of the two-channel model for P_r below 0.95 is illustrated with real engine data.



(a) Comparison between the model and the measurements for different throttle openings (19.00, 20.00, 21.00, 22.50, 25.00, 27.50, 30.00, 35.00, 40.00, 50.00, 60.00, 77.00 deg.)



(b) Relative air mass flow error



(c) Comparison between the model and the measurements for different engine speeds (from 2000 RPM to 4000 RPM in steps of 250 RPM)

Figure 16: Two-channel throttle air mass flow model. Note the large errors (due to pumping fluctuations, as explained in the main text of this paper) for pressure ratios close to 1. These results are from real engine data.

B The engine model used for the simulations

A sketch of the engine model used for all the simulations is shown in Figure 17. The most important dimensions can be read directly from the figure.

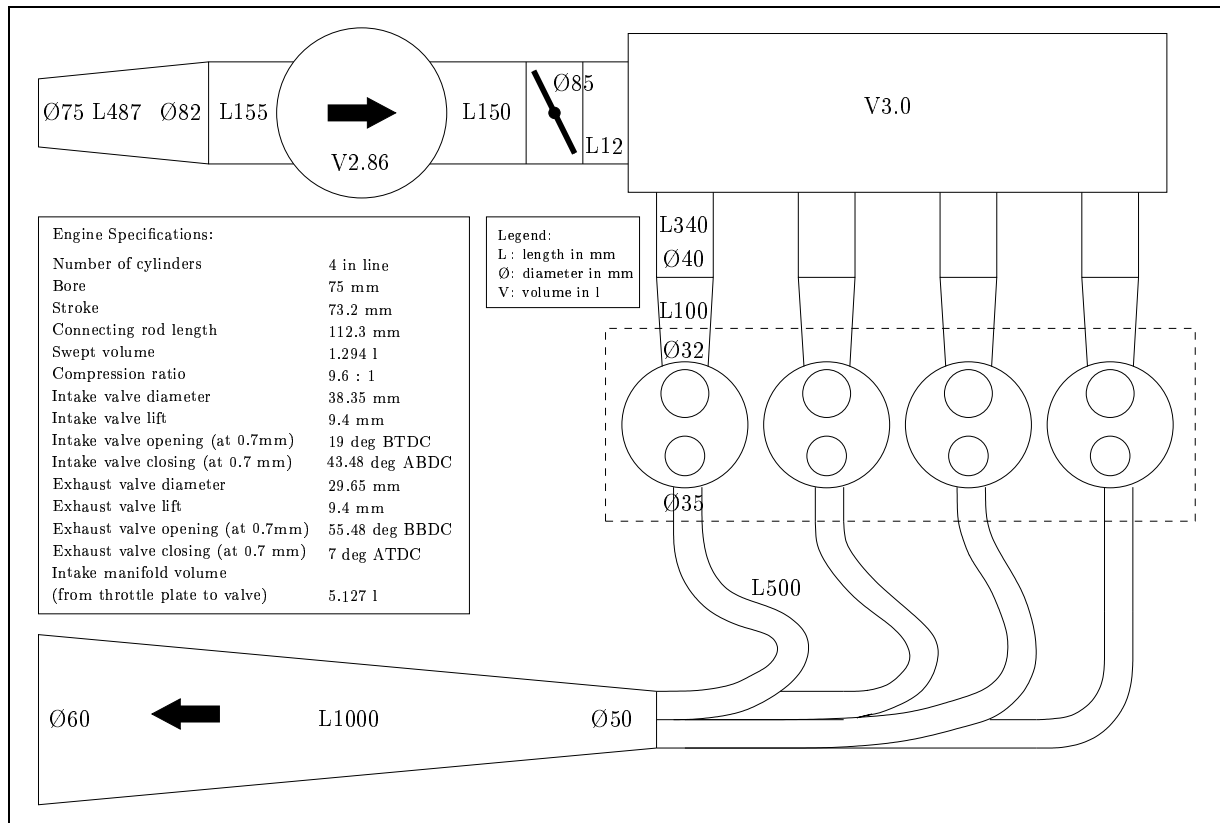


Figure 17: Schematic representation of the simulated engine.